

	nBLM Project – CDR1.2 – report Tests	CEA-ESS-DIA-RP-0047
	ESS-I	

*REPORT*

# NBLM PROJECT – REPORT EXPERIMENTAL TESTS CDR12 FINAL

	<b>REDACTEUR</b> <i>Edited by</i>	<b>VERIFICATEURS</b> <i>Reviewed by</i>		<b>APPROBATEUR</b> <i>Approved by</i>
<b>NOM Prénom</b> <i>Name</i>	SEGUI Laura	PAPAEVANGELOU Thomas		PAPAEVANGELOU Thomas
<b>Date et signatures</b> <i>Date and visas</i>				

 	nBLM Project – CDR1.1	CEA-ESS-DIA-RP-0047
	ESS-I	Page 2 sur 40

<b>CARTOUCHE D'ÉVOLUTION - DOCUMENT REVISION HISTORY</b>			
<b>Éditions</b> <i>Editions</i>	<b>Dates</b> <i>Dates</i>	<b>§ modifiés</b> <i>Modified part(s)</i>	<b>Commentaires –</b> <i>Observations</i>
A		Tous	Création

<b>LISTE DE DIFFUSION – DISTRIBUTION LIST</b>	
<b><u>Interne - Internal :</u></b> - nBLM team	<b><u>Externe - External :</u></b> - ESS
Copies – Copy to :	

## CONTENTS

<b>1. Introduction</b>	4
1.1. Purpose	4
1.2. List of tests	4
<b>2. Response and calibration studies</b>	5
2.1. Efficiency and geometry optimization	6
2.1.1. Slow nBLM	6
2.1.2. Fast nBLM	7
2.1.3. Convertor comparison	8
2.2. First proof of neutron/gamma rejection	8
2.3. MonteCarlo Comparison	9
<b>3. Response to gammas</b>	11
<b>4. Response to thermal neutrons</b>	11
<b>5. Signal characteristics for different drift distances</b>	15
<b>6. B4C Thickness</b>	16
<b>7. Response in accelerator conditions</b>	17
7.1. MC40	17
7.2. IPHI	18
7.3. LINAC4	21
7.3.1. Results	21
7.3.2. Beam losses at Linac4	25
7.3.3. FEE response	32
7.3.4. DAQ response	33
<b>8. HV and LV modules stability</b>	34
References	40

## 1. Introduction

### 1.1. Purpose

This document intends to complement CDR12 package. The aim is to summarize all the tests done with the nBLM prototypes to proof their concept, optimize the geometry and study the response of the detectors, the FEE and the DAQ in real accelerator conditions.

The list of tests performed at different irradiation facilities are summarized in Table 1. Results are discussed in the following section not necessarily in chronological order. Other tests performed in the lab with a  $^{252}\text{Cf}$  source have been also presented before in CDR11 and are not discussed here. They include the study of the use of a long signal cable [1]. Some of this results have been also shown in [2]. The analysis is explained in Appendix A.

### 1.2. List of tests

Installation	Date	Goal of test	Results	Figure(s)
MC40 (Birmingham)	Nov-17	First test in an accelerator	Linear response with beam current	Figure 15
IPHI (Saclay)	Jan-18	First test in a beam pulsed accelerator First test of FEE in accelerator First test of fast module with big neutron flux	Time Response Neutron identification (FEE test) Algorithm development	Figure 16, Figure 17, Figure 18, Figure 19, Figure 20
AMANDE (Cadarache)	March-18	Calibration of detectors Moderator optimization Fast module tested at high energies First gamma/neutron discrimination	Response curves as a function of moderator thickness and neutron energy	Figure 1, Figure 2, Figure 3, Figure 4, Figure 5, Figure 6
ORPHEE (Saclay)	March-18	Response to thermal neutron B4C thickness studies	Response to thermal neutrons Signal characteristics B4C thickness studies	Figure 8, Figure 9, Figure 10, Figure 12, Figure 13
LINAC4 (CERN)	Oct/ Dec-18	Test in real accelerator conditions Test the FEE, the DAQ and the detectors	Response to beam losses Response to gammas from RF	Figure 29
Saclay	Jan-19	Detailed study neutrons vs gamma Test of one final nBLM module	Gain curves Discrimination n/gamma	Analysis on-going

**Table 1:** List of irradiation facilities and tests performed in each one with the nBLM prototypes and the nBLM pre-series to study their response.

## 2. Response and calibration studies

The detectors were tested with monoenergetic neutron fluxes in the AMANDE installation at CEA-Cadarache in the South of France. It is an installation with monoenergetic neutron reference fields.

The goal was to perform:

- Absolute efficiency measurements
- Comparison with Geant4 simulations
- For the Slow module
  - Polyethylene thickness optimization
- For the Fast module:
  - Convertor comparison
- Extra: gamma rejection proof

The measurements were performed using a slow electronics: charge preamplifier + shaper and amplifier to be able to compare with Cadarache analysis directly. A shadow cone was used for neutron backscatter suppression. IRSN reference detectors were used for precise measurement of the flux. In all measurements the fluence was  $>10^4$ - $10^6$  n cm<sup>-2</sup>.

Tests are summarized in Table 2. The measurements for the slow have been repeated for 4 different polyethylene thickness (3, 4, 5 and 7 cm). We had an extra run with only a gamma field. Three acquisition systems have been used: the AMANDE system, a multi-channel analyzer and a high rate sampling oscilloscope, obtaining compatible results in all cases.

Detector	Neutron-to-charge convertor		Drift distance	Neutron energies (keV)				
	Slow	1.5 μm B4C		0.4 mm	565	1200	2500	5000
Fast	Mylar 100μm	Polypropylene 1mm	2mm	565	1200	2500	5000	14800

**Table 2:** Summary of energies studied in AMANDE and characteristics of each nBLM module used for each one. The measurements for the slow have been repeated for 4 different polyethylene thickness (3, 4, 5 and 7 cm).

## 2.1. Efficiency and geometry optimization

### 2.1.1. Slow nBLM

Results obtained with the slow module are shown in Figure 1. In them the efficiency is plotted versus the initial neutron energy and versus the polyethylene thickness. The spectrum of the expected neutron energies from losses simulated at ESS is peaked around 1 MeV [3]. For this energy an efficiency of  $\sim 0.25\%$  is expected if we use 5cm polyethylene. This efficiency corresponds to about a count rate of few c/s for a neutron fluence rate of 1/s/cm<sup>2</sup>.

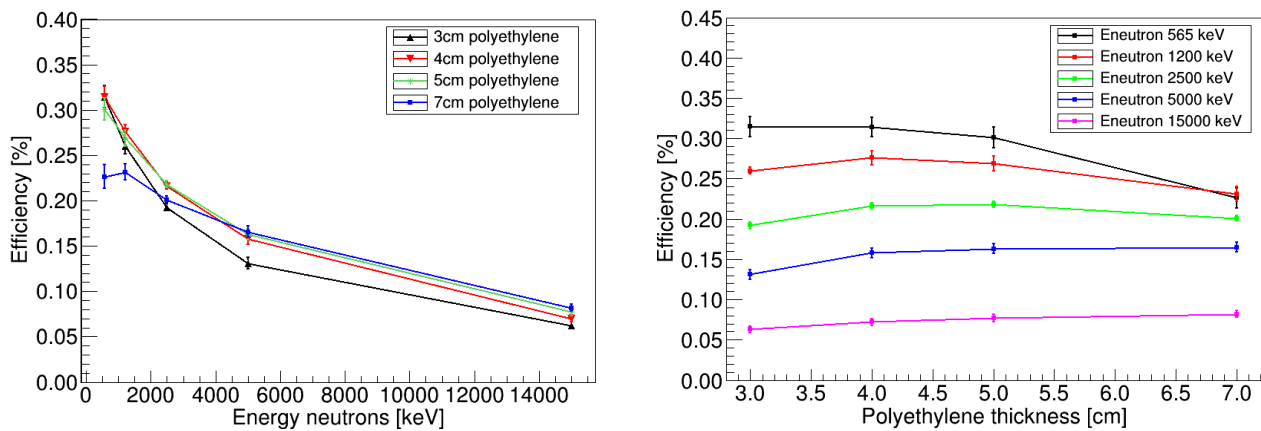


**Figure 1 :** Efficiency of the slow nBLM module with respect to the neutron energy (left) and with respect the polyethylene thickness

### Efficiency with respect the energy threshold

In the case of the slow module, the reaction in the convertor is (n, alpha) [4] conversion with the alpha always of the same energy, i.e. we have an alpha energy distribution as shown in Figure 2. In this case then, we have a small dependency with the energy threshold as shown in Figure 2.

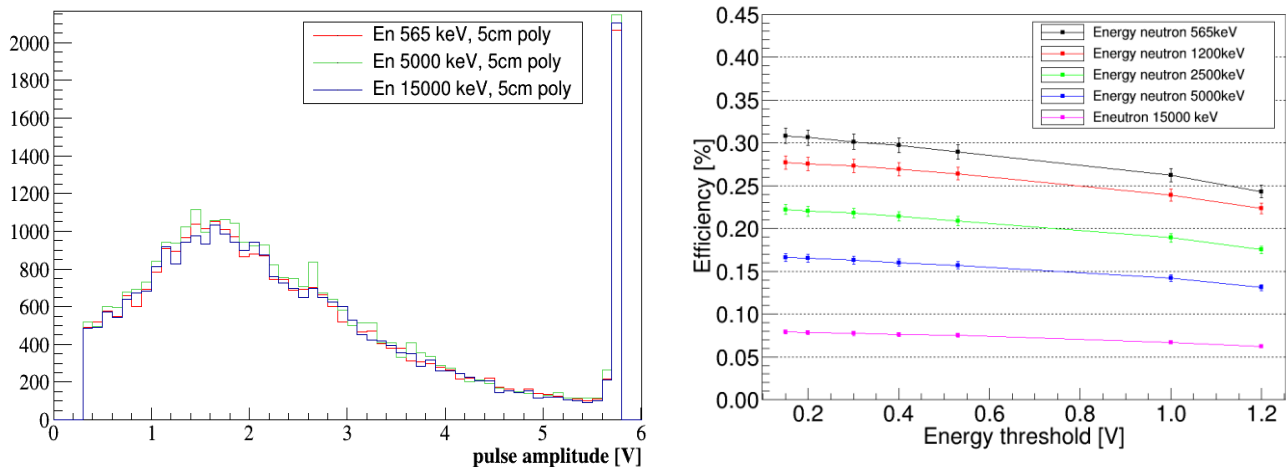


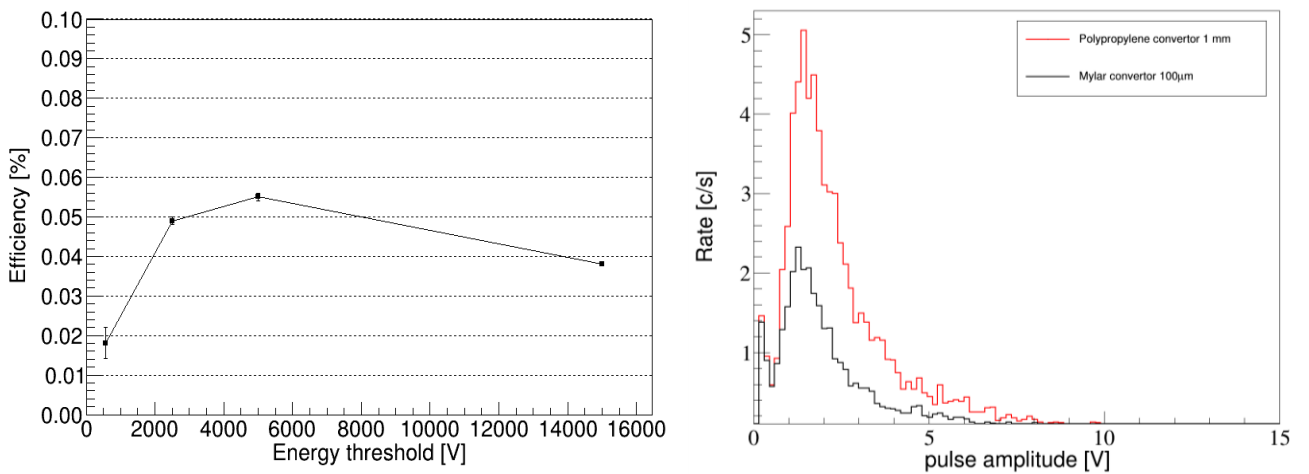
**Figure 2 :** Energy spectrum measured with the slow module for different neutron energies (left). Dependency of the efficiency with the energy threshold.

**Conclusions:**

- Polyethylene thickness fixed at 5cm. No big difference between 4 and 5 cm and for practical reasons we chosen 5 cm (the polyethylene blocks were already of this size in the supplier).
- Count rate of few c/s for a neutron fluence rate of 1/s/cm<sup>2</sup>
- Small dependency with energy threshold

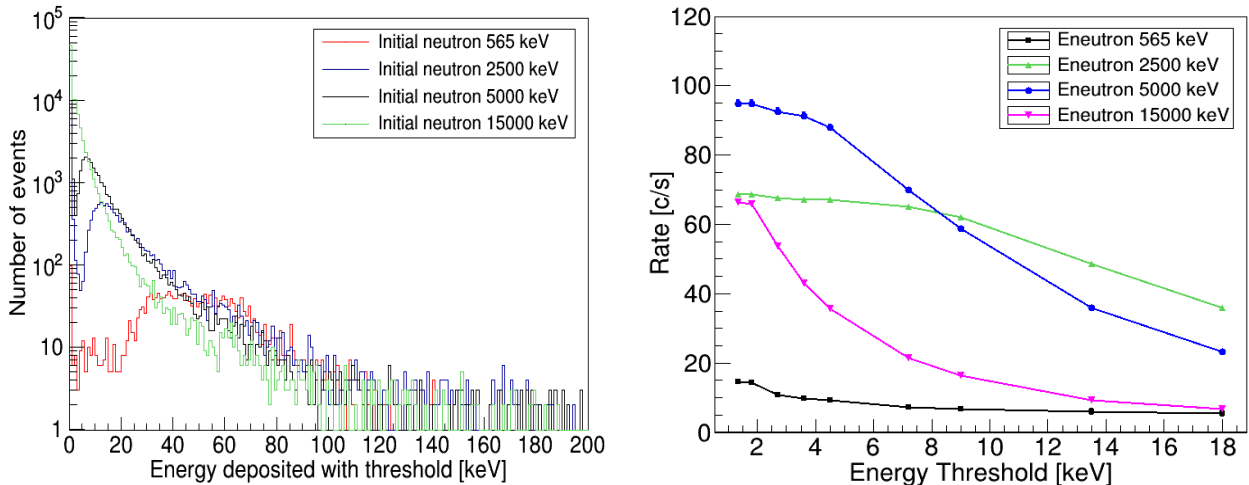
**2.1.2. Fast nBLM**

For the fast nBLM module, results are shown in Figure 3 left. However, in Figure 5 we can also see the strong dependency with the energy threshold. In this case the values in Figure 3 left are for energy threshold of ~0.32V corresponding to ~2.8 keV.





**Figure 3 :** Efficiency of the fast nBLM module with respect to the neutron energy (left) and amplitude spectrum for two different convertors (right)

**Efficiency with respect the energy threshold**



**Figure 4:** Energy spectrum measured with the fast module for different neutron energies (left). Dependency of the efficiency with the energy threshold.

 	nBLM Project – CDR1.1	CEA-ESS-DIA-RP-0047
	ESS-I	Page 8 sur 40

In the case of the fast module, what we detect are the protons emitted in a inelastic scattering (n,p) [4] in the convertor. The produced protons, that will ionize the gas, are emitted with a continuum of energies. For certain energies, they have a preferred energy of emission and produce a kind of a peak as can be seen in Figure 4 left. However, in the case of a white neutron source this will be erased and we will have a continuum of energies. For this reason, in the fast module, the dependency of the efficiency with the threshold is stronger as can be observed in Figure 4 right.

### 2.1.3. Convertor comparison

We took data with two different convertors as indicated in Table 2. Only a factor 2 difference between using polypropylene or mylar as convertors as can be seen in Figure 3 right. Mylar is already metallized and is easier to apply the HV to the cathode with it. For those reasons was chosen over polypropylene.

#### Conclusions:

- Efficiency strongly dependent
  - on threshold
  - on initial neutron energy
- Efficiency between factor 5-20 smaller than slow module (as expected)
- Only a factor 2 difference between using polypropylene or mylar as convertors. Mylar easy to manufacture and is already metallized already in order to apply the HV to the cathode. For those reasons was chosen over polypropylene.

## 2.2. First proof of neutron/gamma rejection

In the case of the 565 keV neutron field, a LiF target was used to produce the neutrons. There is therefore a contamination by the 6-7 MeV gammas coming from the  $^{19}\text{F}(p, \alpha)^{16}\text{O}$  reaction. By using an  $\text{AlF}_3$  target with the same thickness of fluorine, it is possible to isolate the response of the detector to gammas compared to the mixed field. The results are shown in Figure 5 for the fast and in Fig. 8 for the slow detector. Even though that 565 keV is very close to the lower limit of the sensitivity of the fast detector, it is clear that applying a threshold in the pulse amplitude it is possible to completely suppress the gammas while maintaining a good efficiency for the neutrons. As mentioned before, this suppression is an intrinsic characteristic of the detector and is due to the much higher ionization power of the proton recoils compared to the electrons that are produced by the gammas. It can be optimised with the choice of the operating voltages, the gas and the drift gap.

In the case of the slow detector the suppression is even stronger, because the ionization is caused by the  $\alpha$  or  $^7\text{Li}$  particles emitted by the  $^{10}\text{B}(n, \alpha)^7\text{Li}$  reaction. This allows us to reduce the drift gap (it was 0.4 mm compared to 2 mm for the fast) and the detector gain, suppressing thus the gammas even further. In parallel, since most of the reactions are caused by thermalized neutrons, the same suppression factor is possible independently of the initial energy of the incoming neutron.



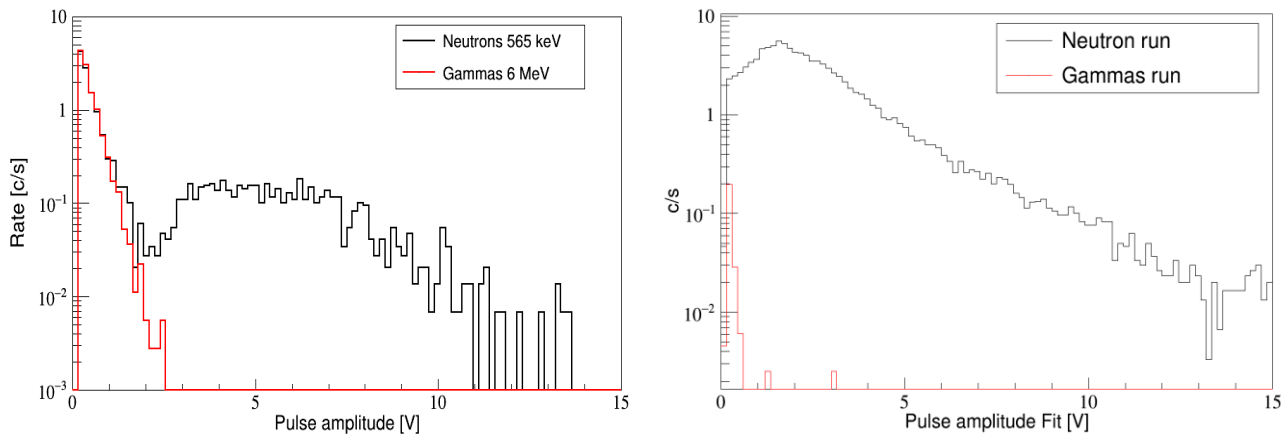


**Figure 5:** Response of the fast detector to the gammas from the  $^{19}\text{F}(p, \alpha)^{16}\text{O}$  reaction and to the mixed field of gammas and 565 keV neutrons. (Right) Same for the slow module.

The rejection is due to the difference in the ionization power between protons/alphas and electrons. The choice of He gas enhances this suppression. With an energy threshold we can totally reject the gamma contribution. The difference in rate observed between fast and slow due to different drift distance (1.9 mm in fast / 0.4 in slow). For the final design, however, a distance of 2 mm drift have been chosen. This gives a larger possible gain range without sparks, while the gamma contribution remain very small.

### 2.3. MonteCarlo Comparison

The results obtained allow also the comparison with the simulations performed in Geant4 to validate the simulation framework. In both cases, the agreement is very good. In the case of the fast however, there are some qualitative discrepancies that are still under investigation. As previously mentioned, the effect of the threshold is much higher and this could be one of the reason of the differences observed.

In the case of the slow we can see a comparison of the energy spectrum in Figure 6 left. For the comparison of the energy spectrum we have compared the histograms bin by bin and use the chi2 test from ROOT for different calibration factors. We have assumed an energy resolution of 30% FWHM at 129 keV. On the right we can see the differences in efficiency comparing data and Montecarlo. From the work of different authors, among them discussions with N.H. Tran from CEA, we know we should include *G4NeutronHPThermalScatteringNames* when defining an element to take into account all the thermal processes. This can explain the differences observed in Figure 6 right. Work is on-going to implement this library and validate the hypothesis. In any case, the differences observed are of less than a factor 2. (Each group of data corresponds to a different neutron energy).

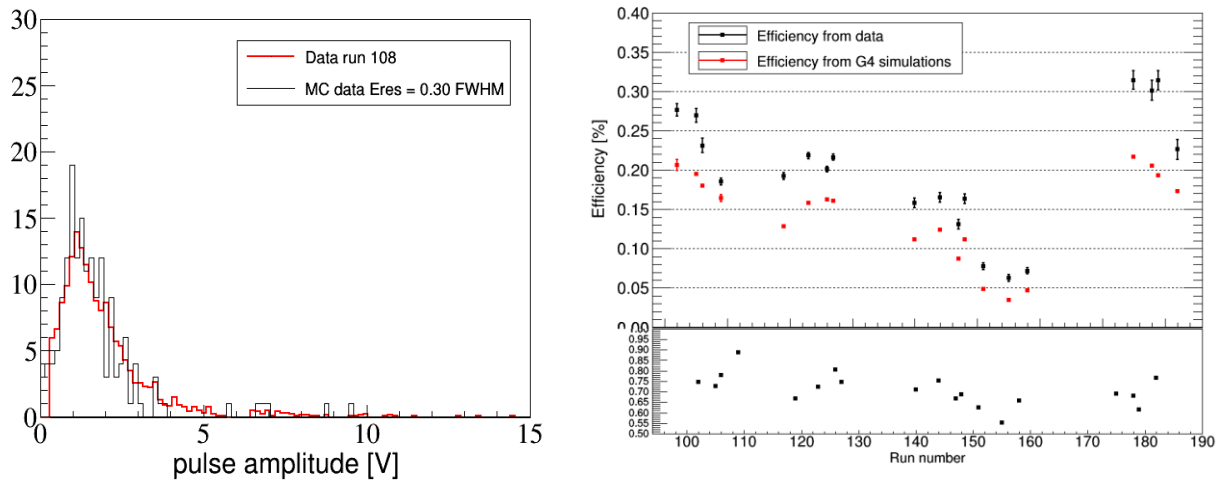


**Figure 6:** Comparison between data and Geant4 simulations for the slow module. (Right) Energy spectrum comparison. (Left) Efficiencies obtained with data (black) and MC (red).

In the case of the fast module, we can see a qualitative comparison in Figure 7.

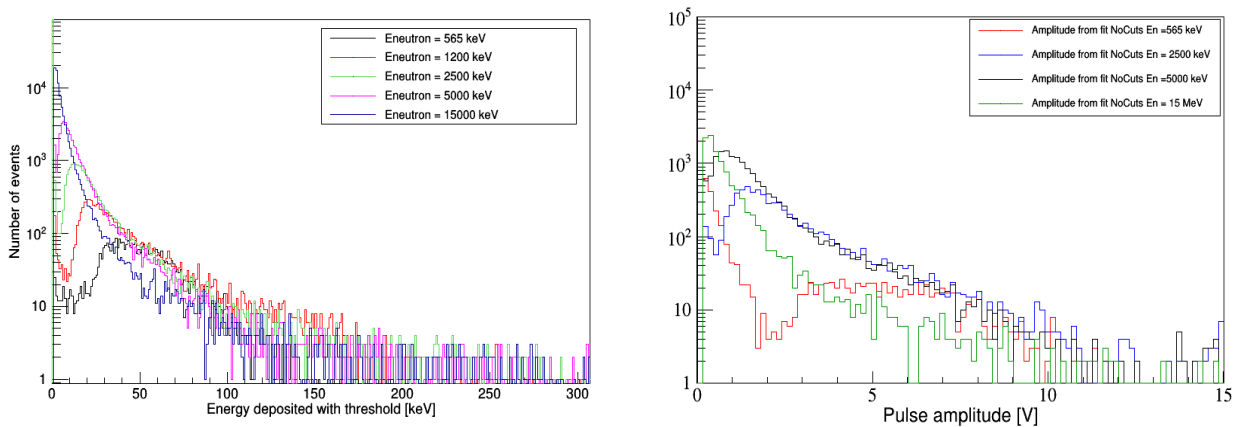
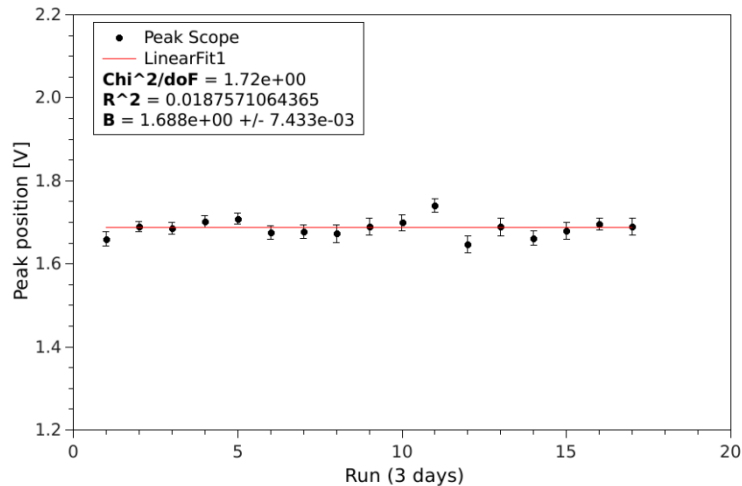


**Figure 7:** Energy spectrum from MC simulation (left) and data (right) for the measurements performed at AMANDE with the fast nBLM module.

We took data for 3 days at the same voltage conditions, so we can see the evolution of the peak in the following image. The peak position was determined by a rough Landau fit to the peak of the slow module.



### 3. Response to gammas

Initial results have been presented in Section 2. More data will be recorded with the first of the final detectors mounted using the final FEE during week 6. Tests will be done with a neutron source ( $\sim 70 \mu\text{Sv/h}$  at 1m) and a gamma source ( $\sim 70 \mu\text{Sv/h}$  at 1m) at CEA-Saclay. The goal is to obtain the gain curve in both cases to define the operation point with the highest rejection to gamma while keeping a high neutron efficiency. Probably preliminary results will be presented during the CDR12 presentations.

### 4. Response to thermal neutrons

Measurements were also carried out in the ORPHEE nuclear reactor, in CEA-Saclay. We performed tests with and without a layer of 5mm Mirrobor in place and with polyethylene alone or polyethylene + 5mm Mirrobor. The summary of the tests is shown in Table 3. The characteristics of the field was neutrons of  $2.2 \text{ \AA}$  (16.9 meV) with a fluence of  $2 \times 10^6 \text{ n/cm}^2/\text{s}$ . All measurements were taken with the fammas electronics reading each of the 4 segments of the Micromegas independently. During analysis we realized that the preamplifiers had different gain two by two. So for the analysis and the following results we consider only half detector to have the same gain.

Drift distance (mm)	B4C (μm)				Mirrobor + B4C (μm)			Polyethylene (7cm)	
	0.2	0.5	1.5	0	0.2	0.5	1.5	B4C (μm)1.5	+ mirrobor 5mm
0.4	✓	✓	✓					✓	✓
1.4	✓	✓	✓	✓	✓	✓			
5.1	✓	✓	✓	✓	✓	✓			
10.2			✓						

**Table 3:** List of tests performed at ORPHEE (nuclear reactor)

Data was recorded in same conditions with or without 5 mm Mirrobor in front of the detector. There are two set of data as listed in Table 4: run 231 and run 234 were taken in same conditions with the difference of placing the mirrobor or not, the second set is run 239 and 240. In both cases we obtain a reduction factor of  $\sim 2.5 \times 10^{-4}$ . Results are shown in the and in Table 4 and in Figure 8, Figure 9 and Figure 10.

We show the rate calculated in two different ways and the rate evolution. The details of the analysis are described in Appendix A. Moreover, we study the shielding including also polyethylene, as it will be the case for the slow module (the only one sensitive to thermal neutrons).

Run	Voltages	Drift	B4C	Mirrobor	Poly.	Rate
231	Vm = 500V	1.4	0.2			$(3.09 \pm 0.29) \times 10^4$
234	Vd = 640V			✓		$1.38 \pm 0.09$
239	Vm = 500V	5.1	0.2			$(3.58 \pm 0.02) \times 10^4$
240	Vd = 1010V			✓		$1.47 \pm 0.07$
Background	Several runs					$1.00 \pm 0.05$
203	Vm = 475V Vd = 515V	0.4	1.5		✓	$134.95 \pm 10.49$
204				✓	✓	0.4
205						$(3.81 \pm ) \times 10^5$

**Table 4:** Runs with and without mirrobor to study the response to thermal neutrons

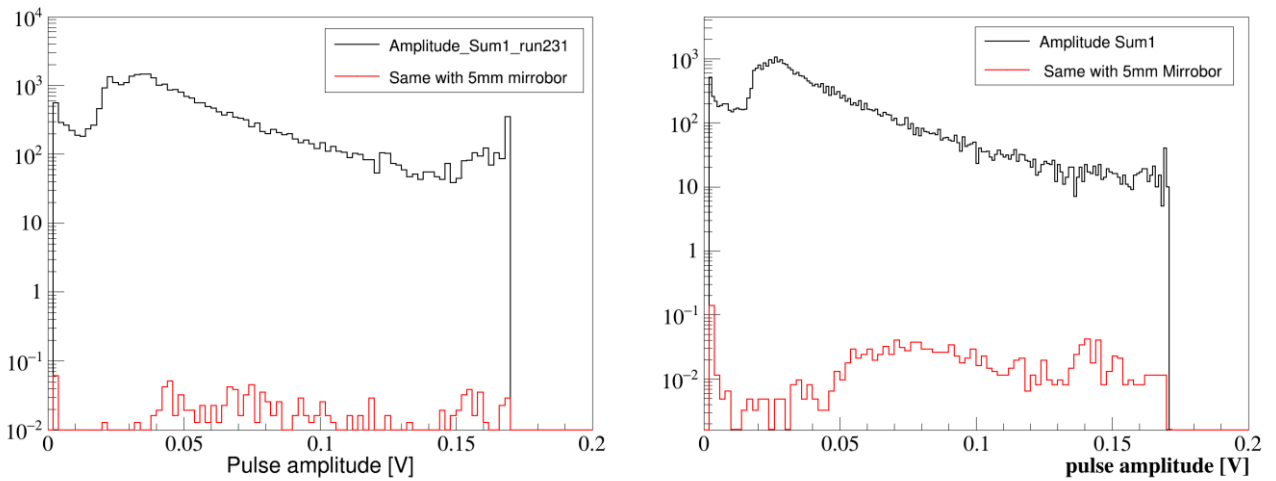


**Figure 8:** Amplitude spectrum for the two set of data used top study the effect of mirrobor as list in Table 4. (Right) comparing runs 231 and 234 and (left) comparing runs 239 and 240. In both cases in red is the results with mirrobor in place and in black without it.

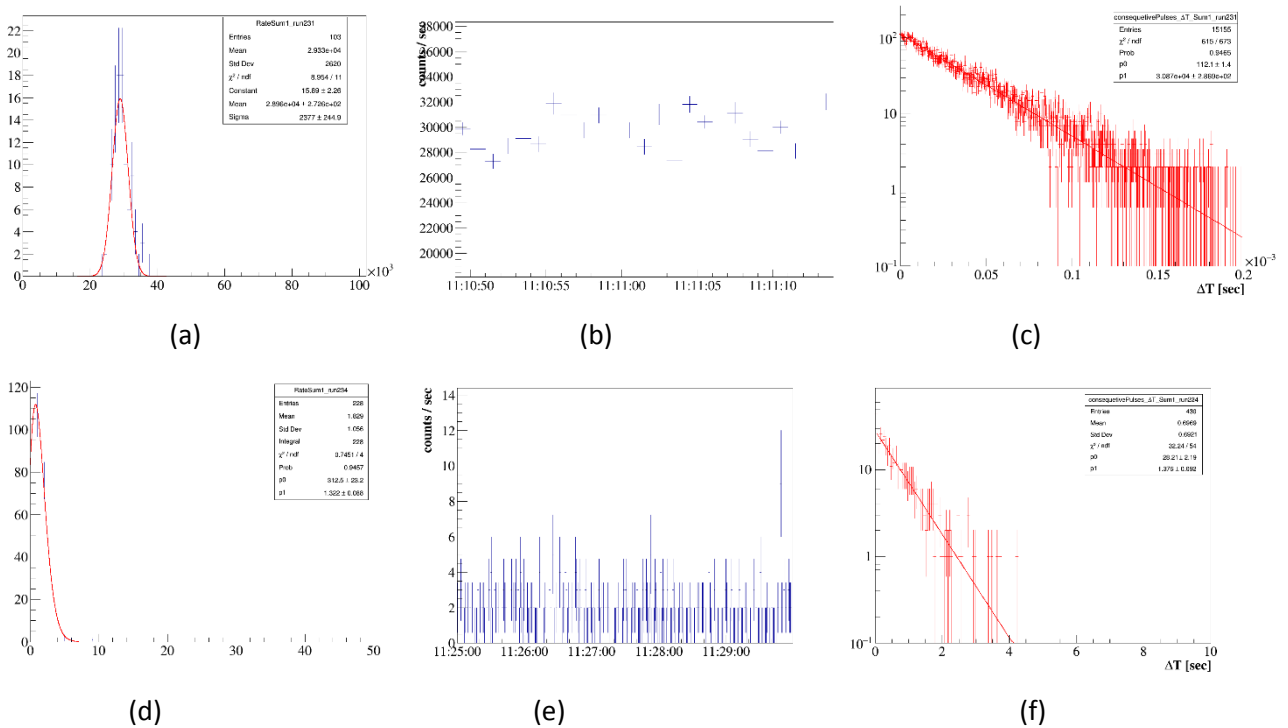


**Figure 9 :** (a) Rate Distribution (b) Rate evolution (c) Time difference between consecutive events to obtain the rate (more in Appendix A) for the run without mirrobor (run 231). (d), (e) and (f) same but with 5mm Mirrobor in place (run 234).

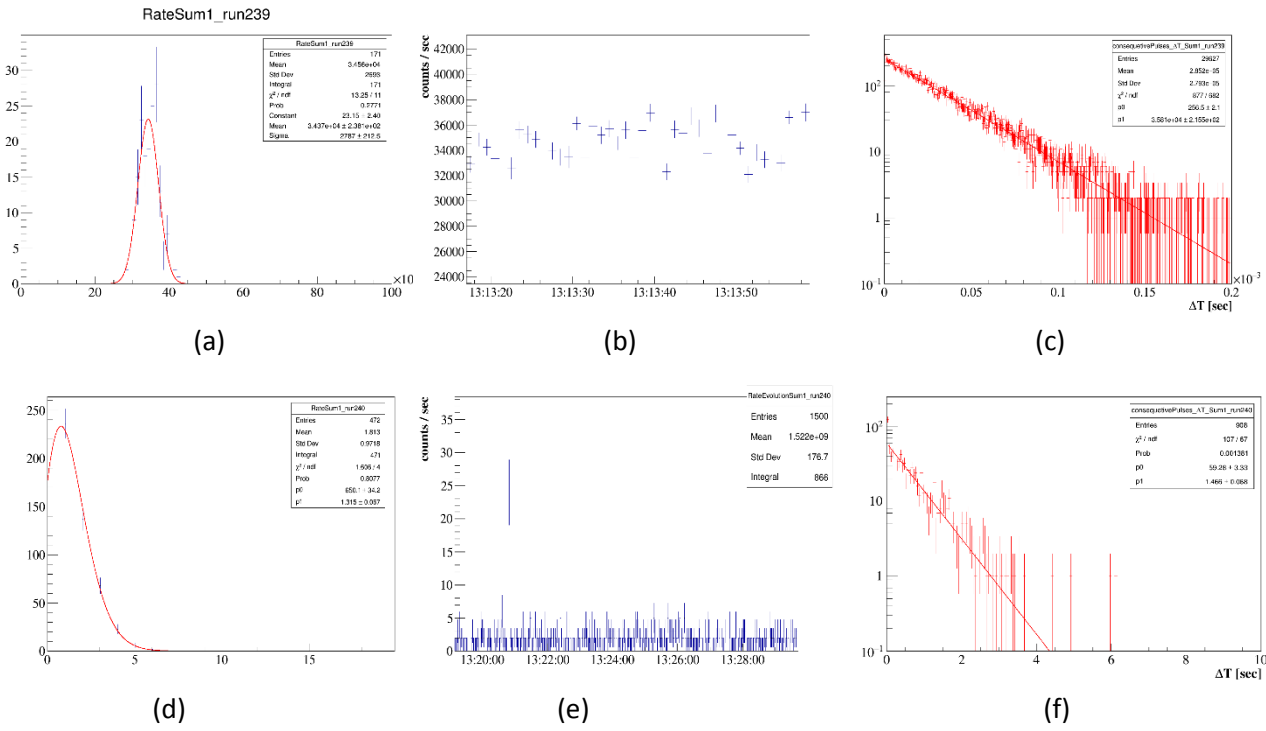


**Figure 10 :** (a) Rate Distribution (b) Rate evolution (c) Time difference between consecutive events to obtain the rate (more in Appendix A) for the run without mirrobor (run 239). (d), (e) and (f) same but with 5mm Mirrobor in place (run 240).

Until now, we have evaluated the effect of Mirrobor alone, but in the installation we will have 5 mm Mirrobor + 5 cm polyethylene. Unfortunately the data was taken with 7 cm polyethylene but we can see the extra rejection of the polyethylene alone and for the polyethylene + mirrobor. Data is in Table 4. With only polyethylene the rejection factor is of  $\sim 3 \times 10^3$  and if we add 5 mm of Mirrobor it is of  $9.5 \times 10^5$ .

## 5. Signal characteristics for different drift distances

In ORPHEE, as indicated in previous section, we have also studied the signal shape for different drift distances. The summary of the tests was shown in Table 3.

The rise time and pulse width distributions are shown in Figure 12 for the 4 different drift distances tested: 0.4, 1.4, 5.1 and 10.2 mm. For longer drift distances, the distributions start to be extended. This is due to the alpha particles emitted from the cathode with an angle. The whole charge will take longer to arrive to the Micromegas as sketched in Figure 11. The two “kind” of peaks in the pulse width and rise time are probably due to that in reality in the reaction there are emitted a  ${}^7\text{Li}$  and an alpha.

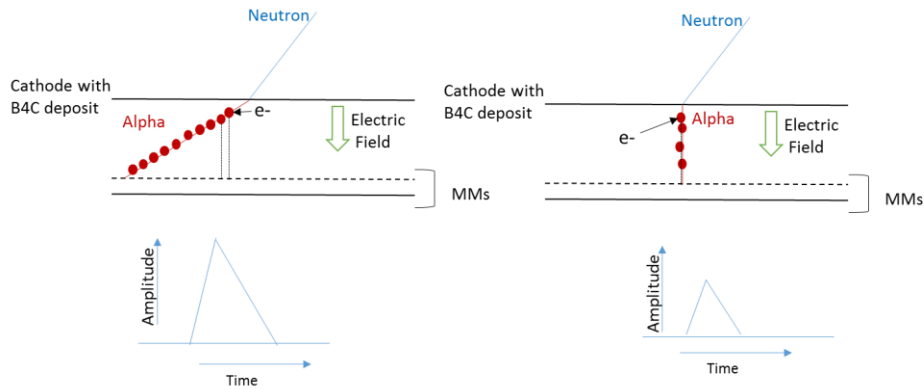


**Figure 11 :** Charge creation and amplitude depending on the alpha emission angle.

Drift distance	Rise Time (ns)		Pulse Width (ns)		Comments
	Mean	Sigma	Mean	Sigma	
0.4	21.03	9.41	70.56	14.62	Values in main peak, but there are like two
1.4	37.84	9.1	113.2	17.68	
5.1			189.8	16.7	
10.2			386.3	22.37	

**Table 5:** Mean value and sigma for the rise time and pulse width for different drift distances.

The mean values and the sigma of the distribution of the rise time and pulse width can be seen in Table 5. Final design will have a drift distance of 2mm that gives a rise time of about 40 ns and a pulse width of 100 ns. However, this distance can be easier modified if needed. 2mm is also safer in terms of sparks than  $\sim 0.5$  mm.

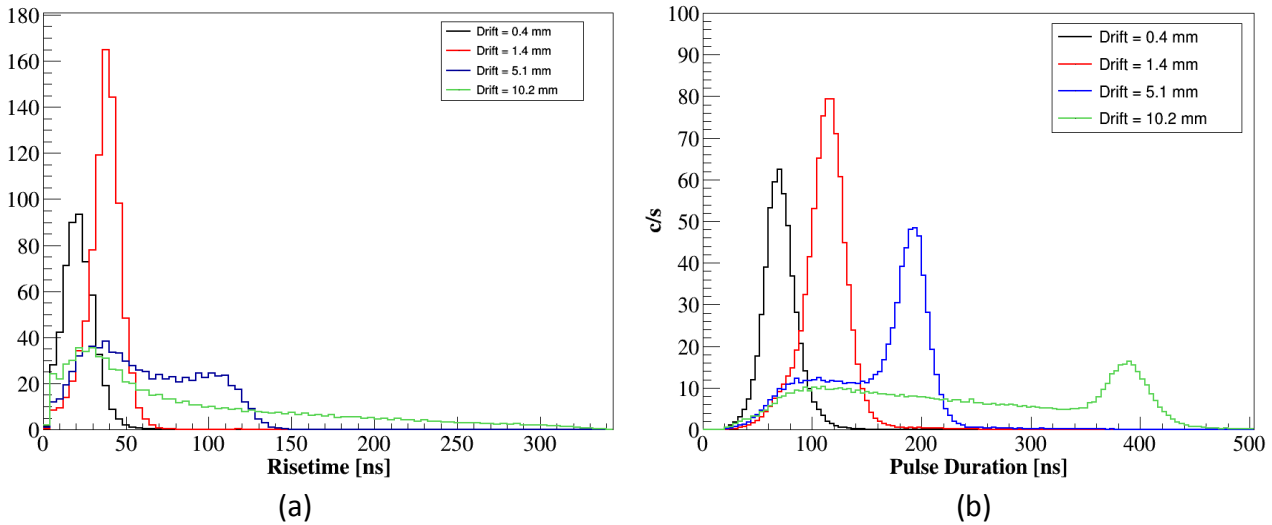


Figure 12: Rise time (a) and pulse duration (b) distributions for different drift distances.

## 6. B4C Thickness

In ORPHEE the response for different  $^{10}\text{B}_4\text{C}$  thickness have been also studied. The summary of the tests was shown in Table 3. Results are in accordance with what expected as can be seen in Figure 13. In the case of the small gap there is no full ionization. We obtain a factor of  $\sim 5$  between 0.2 – 1.5  $\mu\text{m}$ . However, we should indicate here that results are not corrected by the different gain (all measurements were not taken in same field conditions).

For the baseline of the modules we have chosen to use 1.5  $\mu\text{m}$  that gives the maximum efficiency.

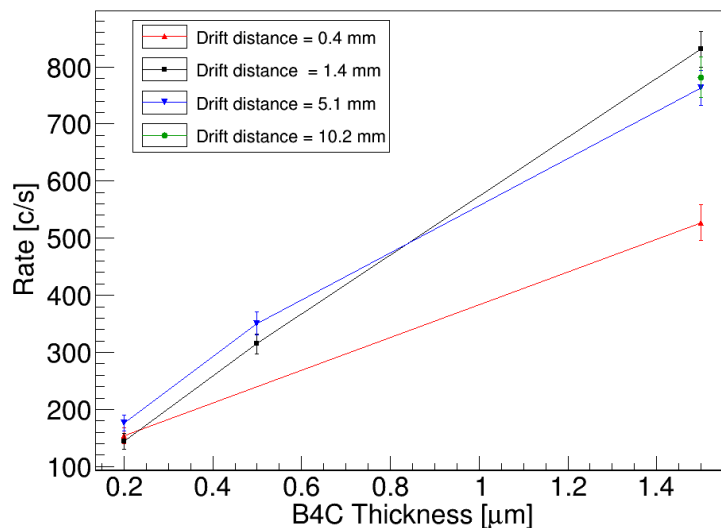


Figure 13: Rate vs  $\text{B}_4\text{C}$  thickness for different drift distances.



## 7. Response in accelerator conditions

### 7.1. MC40

The first test we did in an accelerator was in the MC40 medical synchrotron, in Birmingham, UK. This installation can accelerate protons up to 30 MeV. The beam diameter is  $\sim 1\text{cm}$ . It is a continuum pulse.

Data was taken at 28 MeV and different intensities: 0.017, 0.025, 0.044, 0.051, 0.08, 0.10 nA. We were producing neutrons hitting with the proton beam into an Al plate of  $\varphi=1\text{cm}$ . Tests were performed with the slow module and using a charge preamplifier. The main results was the linear dependency between the proton current and the detected neutron rate Figure 15.

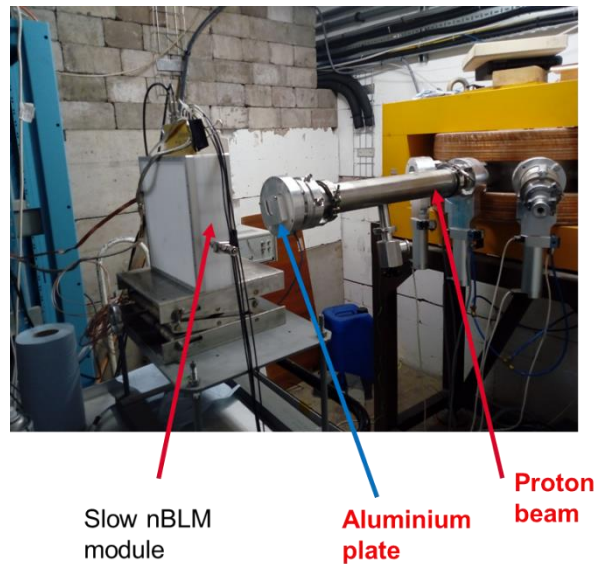


**Figure 14** : Slow nBLM module installed in the MC40 Synchrotron facility.

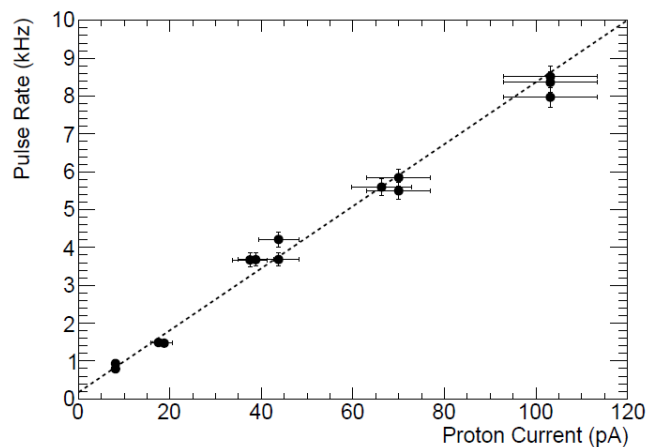


**Figure 15**: Proton beam current hitting in the Al plate vs rate of neutrons detected in the slow nBLM module during the tests performed at the MC40 installation. Analysis performed by K. Nikolopoulos.

## 7.2. IPHI

IPHI is a 3MeV proton accelerator in CEA-Saclay. Several tests were performed in the first quarter of 2018. In part of those tests a Be target was placed to produce a neutron field. Both nBLM prototypes were used in order to measure the neutron flux distribution, but also to study the response of the detectors in a pulsed beam. The energy of the proton beam was 3 MeV and the duration of a pulse about 90  $\mu\text{s}$ , at a repetition frequency of 1 Hz. The data were taken using the FAMMAS amplifiers, who helped us to think about the needs for the analysis and to develop part of the analysis to be implemented in the algorithms in discussions with the CEA-DIS team and ESS-BI team.

### 7.2.1. Time Response

One of the main results was the study of the time response of both modules. Results are shown in Figure 16. The results verified the behaviour predicted by the simulations [5]. The fast detector has an immediate response and the count rate is in direct correlation with the intensity of the beam current, as it was measured in the target (Figure 16 left). In the case of the slow detector, due to the moderation time most of the events are recorded with a delay of 100-200 ns. In the simulated cumulative distribution of the recording time is represented in red, while the measured response to the IPHI pulse is shown in black (Figure 16 right). However, due to the much higher efficiency of the slow detector compared to fast, a significant number of the events ( $\sim 5\%$  of the total) will be register within the first  $\mu\text{s}$ , so also the slow detector can be used for an early warning in case of accidental beam loss.

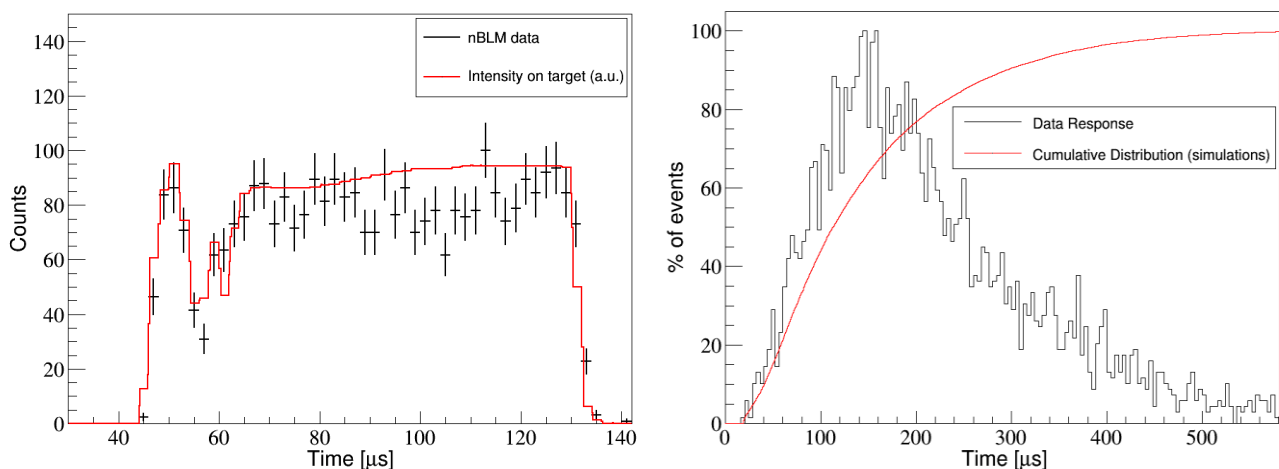


**Figure 16:** (left) Time response of the fast detector (black) in comparison with the intensity of current in the target (red). (Right) Time structure of the events in the slow detector (black) following the 100  $\mu\text{s}$  proton beam pulse. The response is slow due to the moderation time of the neutrons in the polyethylene. The red curve shows the cumulative distribution of the events from a simulated instantaneous pulse.

### 7.2.2. Results single neutrons vs Pile-up

This tests were the first time we record neutrons using the chosen electronics in a high flux environment and thanks to this data we develop our analysis in C and ROOT. During these measurements the 4 segments of the Micromegas were recorded independently by a digital oscilloscope at 250 MS/s (in the final case and in posterior tests performed we have one output channel only). So a more complicated analysis was needed to sum up the 4 channels correcting by offset variations.

As mentioned before data was recorded when using a BE source to produce a high intense neutron field but also when the beam was directly stopped in a Nickel beam dump.

Some examples of the recorded pulses are shown in Figure 17 (with the beam dump), Figure 18 with the Be source in place and in Figure 19 to show the difference in case or not of pile-up in a zoomed region. We can compare in table the counted neutrons in case of pile-up or no pile-up if we rely in the identification of single peak waveforms (Rate) or integrating the charge of the events and dividing by a mean value (RateQ). Those results proof the validity of this method which has been implemented now in the algorithm to implement in the FPGA.

	No pile-up		Pile-up	
	Rate (c/p)	RateQ (c/p)	Rate (c/p)	RateQ (c/p)
<b>SUM Waveform</b>	34.	34.	241	2318
<b>Ch1</b>	OFF	OFF	OFF	OFF
Ch2	12.	11.	518	783
Ch3	10.	10.	521	730
Ch4	7.	6.	473	816

**Table 6:** Obtained rate for the two methods mentioned in the text, direct counting or using the charge method for the case of pile-up or not pile-up.

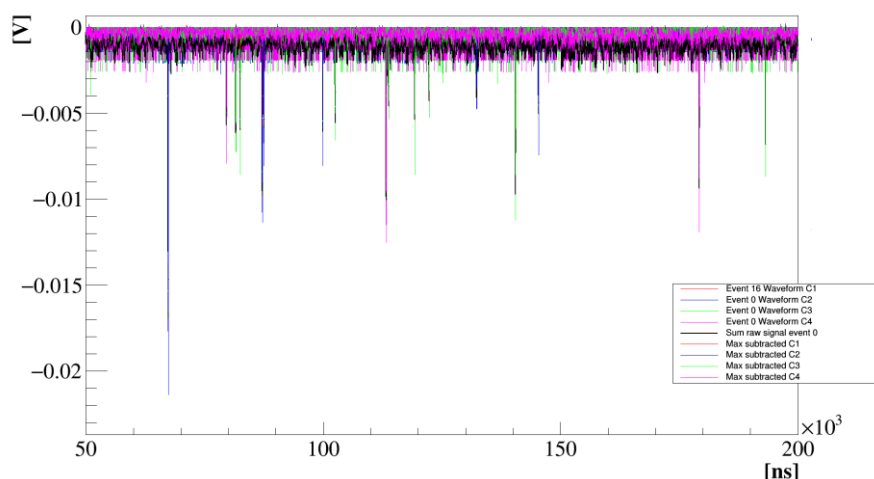


**Figure 17:** Signal from the slow module when the beam was stopped by a Nickel beam dump. Data was registered with an oscilloscope in a time window frame of 2 ms. Each peak corresponds to a single detected neutron. The different colours represent the signal in each of the 4 segments in the Micromegas. And in black is the sum of the 4. Channels offset have been corrected.

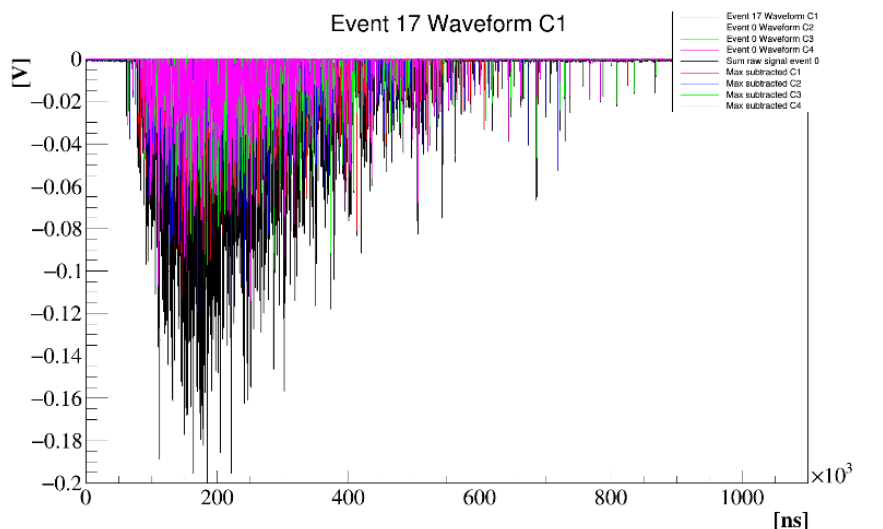


**Figure 18:** Signal from the slow module when the beam hit a Be source to produce a high fluence neutron field. Data was registered with an oscilloscope in a time window frame of 2 ms. Each peak corresponds to a single detected neutron. The different colours represent the signal in each of the 4 segments in the Micromegas. And in black is the sum of the 4. Channels offset have been corrected.

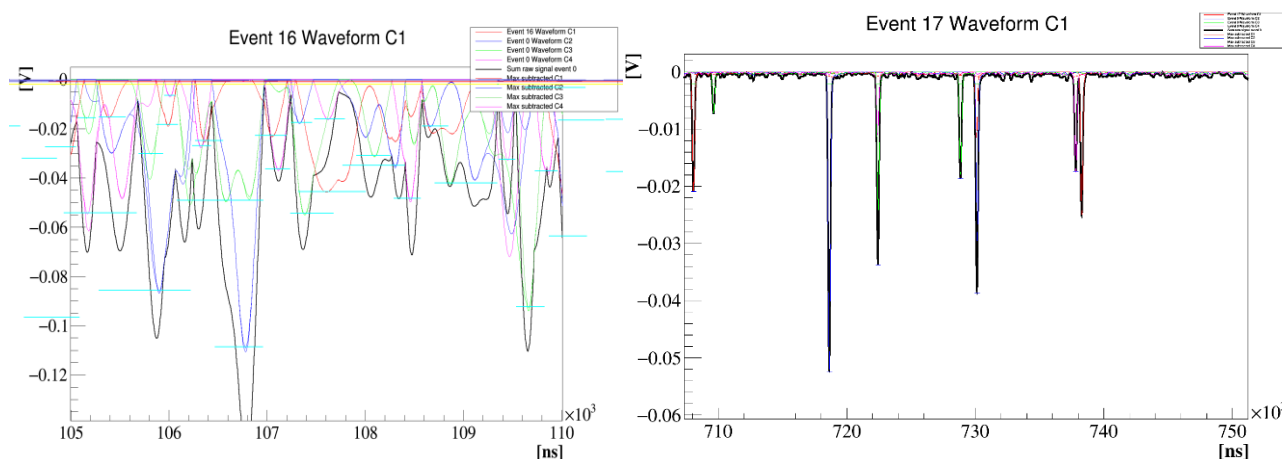


**Figure 19:** (left) Pulse identification in case of pile-up. This corresponds to a zoom in 5µs of Figure 18. (Right) Pulse identification in case of no pile-up.

### 7.2.3. Linear response with beam current

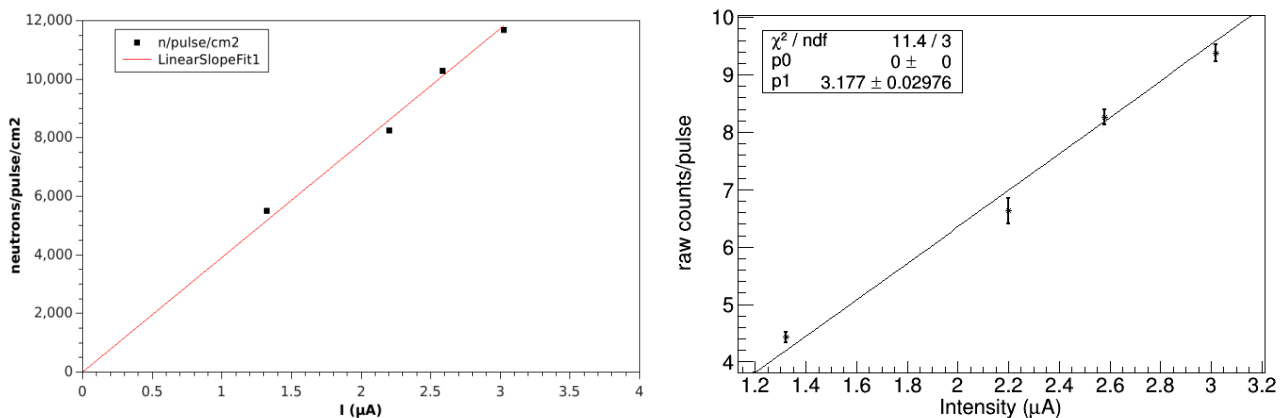


Figure 20: Count Rate vs beam current (for the slow left and the fat right). Y axis in arbitrary units.

### 7.3. LINAC4

A fast nBLM unit was installed at LINAC4 (CERN) in summer 2018. It was installed in the region of about 13 MeV, between two linacs and together with one of the ESS icBLM. An image of the detector installed is shown in Figure 21.

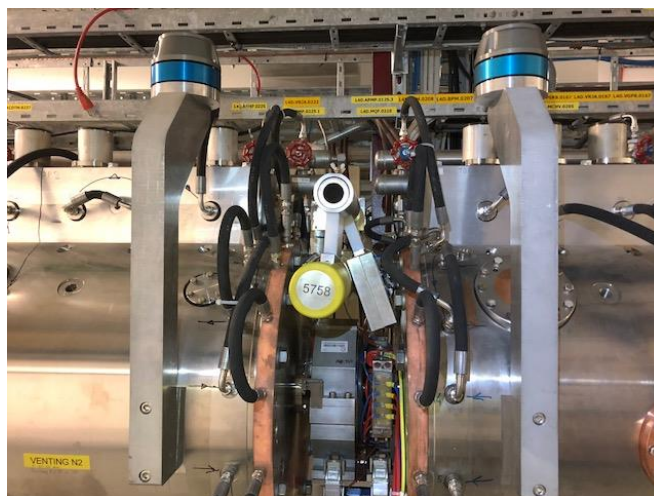
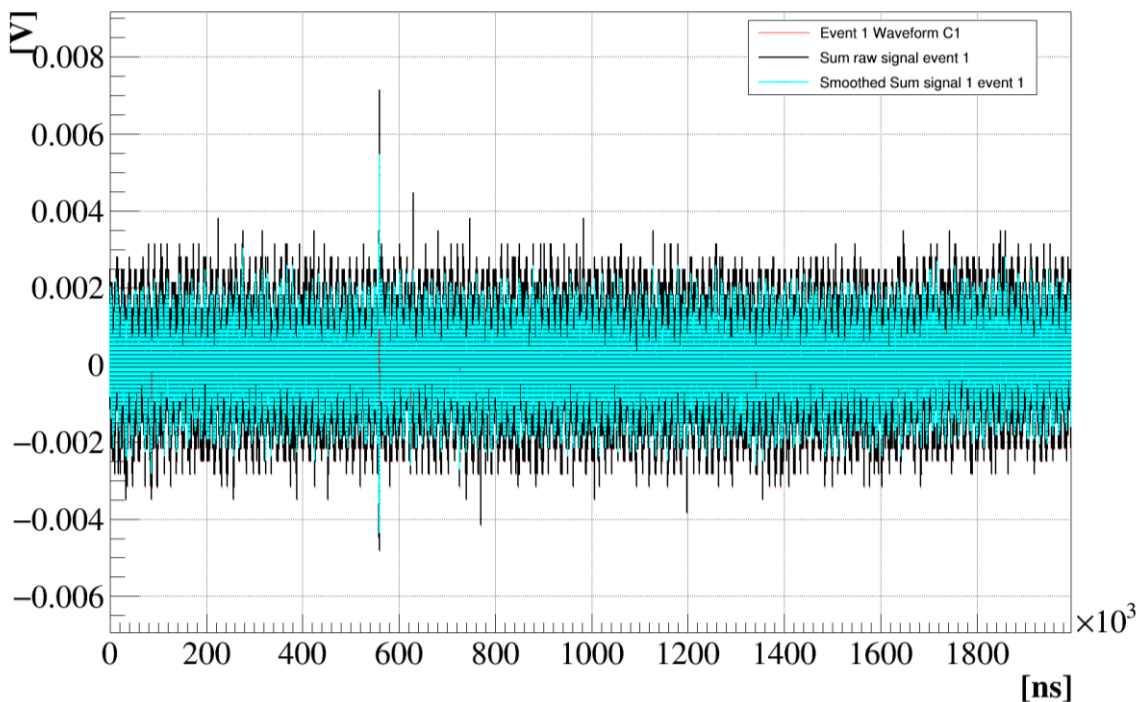


Figure 21: fast nBLM pre-series module installed at LINAC4 (CERN).

#### 7.3.1. Results

Two set of data campaign were done: one in November 2018 and another in December 2018. During the first campaign we understood the behaviour of the detector and test the FMC development for the first time in real conditions. In the second one, beam losses were in purpose produced and clearly identified by our detector. Another test with the FMC newer bit stream version was also performed. Results are presented in [6].

During the first tests, no events or very few, were detected at a gain of  $\sim 500$  V in the mesh. An example is shown in Figure 22. The detector was installed and connected to the gas line by the Linac4 team, as we had no access to the tunnel, three months before we start the tests, so it was difficult to be sure about the detector and gas status. Therefore, we decided to increase the gain to force some sparks to check if the detector was alive. This did not happen until 575 V. At a high gain of  $\sim 550$  V ( $\sim 50$ - $75$  V higher than the measurements done until the date) we start to detect much more events (Figure 23). They were distributed in a beam duration of  $\sim 720\mu\text{s}$ , approximately the RF pulse duration. We have realized indeed that we were detecting gammas from the RF and very few neutrons (higher amplitude events) when operating at high gain. Based on the measurements performed before we consider nominal operation conditions when  $V_m = 475$ - $500$ V and the voltage in the cathode is  $<1200$  V.



**Figure 22:** Pulses detected with an oscilloscope when operating the nBLM fast module at low gain in the mesh (500 V). Data was recorded with a fast oscilloscope at a sampling of 4ns in a 2000  $\mu\text{s}$  window.

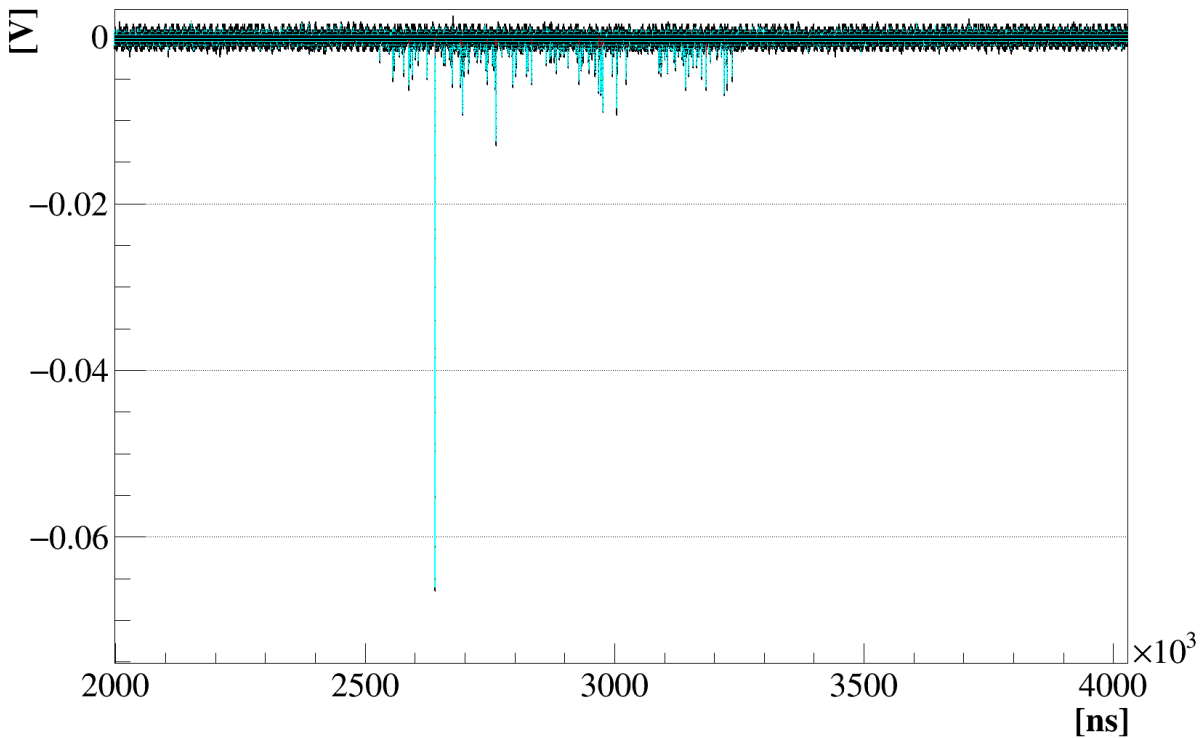


**Figure 23:** Pulses detected with an oscilloscope when operating the nBLM fast module at high gain (550 V). Low amplitude peaks, distributed in a length of about 700  $\mu$ s are gammas emitted from the RF. The only high amplitude event is more likely to be a neutron. When selecting only high amplitude events they are distributed in a pulse of  $\sim$ 150  $\mu$ s, what corresponds with the beam pulse, as is shown in Figure 24. Data was recorded with a fast oscilloscope at a sampling of 4ns in a 5000  $\mu$ s window.

As the rate of neutrons was very low, we took a long run triggering in high amplitude events instead of triggering with the accelerator. The information of the accelerator trigger was also saved and therefore, each event is corrected during analysis with the accelerator trigger. This run corresponds to run 412 and data was taken during  $\sim$ 6h. In Figure 24 the pulse amplitude (left) and the beam time structure (right) for run 412 is shown. The different colours corresponds to different energy cuts. We can see that selecting events with an amplitude  $>$  30 mV (red curve) the beam structure decreases to  $\sim$ 170  $\mu$ s, which corresponds to the beam pulse duration. If, on the contrary, we select all events above the noise threshold (2.5mV, black curve), the beam time is  $\sim$ 750  $\mu$ s, which corresponds to the RF pulse. We can also see how the events below  $\sim$ 20 mV fit quite well to an exponential which is the expected shape of the gammas energy distribution as obtained from the simulations [3]. In next section, we will compare the amplitude distribution for a run operating at high gain with a run at a gain closer to what we expect to be the nominal operation conditions.

Data at different voltages for gammas and neutrons will be recorded during week 6 at Saclay to obtain a gain curve to determine the best operation point. We should also note that during this data taking, different tests were performed in the accelerator as they were commissioning the machine, so we are not completely sure about the conditions some of this data was taken.



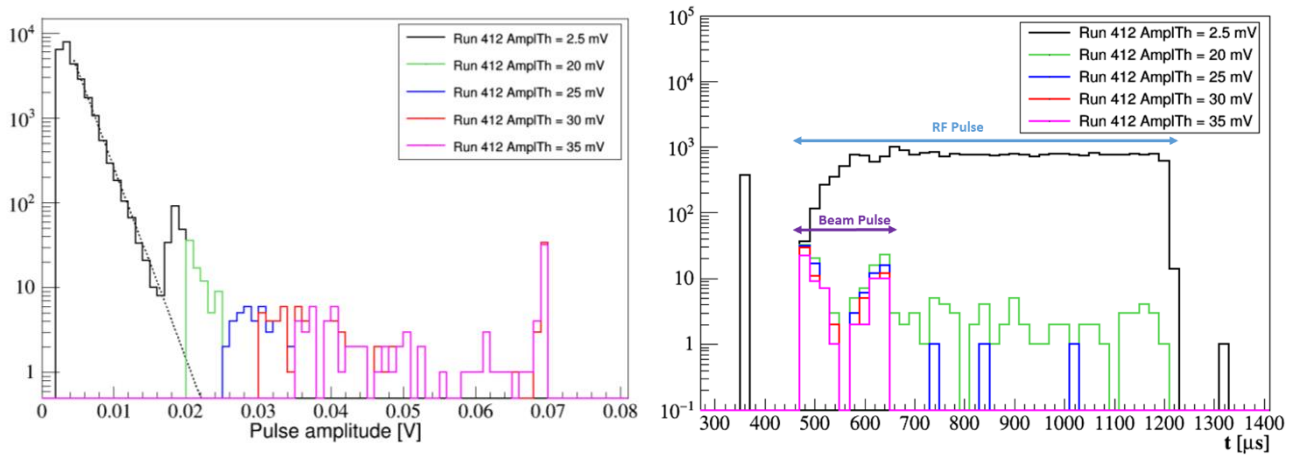


**Figure 24:** Pulse amplitude (left) and beam time structure (right) for run 412. This run was taken with trigger in high amplitude events, what we think are neutrons. Different colours corresponds to different energy cuts. We can see than selecting events with an amplitude  $> 30\text{mV}$  (red curve) the beam structure decreases to  $\sim 170\ \mu\text{s}$  (counting from  $\sim 470\ \mu\text{s}$ , where our time offset is), which corresponds to the beam pulse duration. If, on the contrary we select all events above the noise threshold ( $2.5\text{mV}$ ), the beam time is  $\sim 750\ \mu\text{s}$ , which corresponds to the RF pulse.



### 7.3.2. Beam losses at Linac4

In December 2018, a second data campaign was performed. During this time, uniform beam losses, continuously produced, were forced. They were done sending the beam completely down everywhere at the level of MEBT. Several runs are discussed in this section and they are listed in Table 7.

Run	Vm	Vd	Neutrons Amp Th (mV)	Neutrons Q Th (a.u)	Comments
413	550	1500	11	3.0	1 <sup>st</sup> provoked (and detected) losses
414	525	1000	6	1.2	No losses
415	525	1000	6	1.2	Losses
420	550	1500	30	7.0	Losses, long run over night in autotrigger mode

**Table 7 :** Voltages in mesh and drift for the runs taken at Linac4 during December 2018 and discussed in this section. The amplitude and charge thresholds used to select neutrons are also indicated.

Most of the runs are of few minutes duration but we took a long run (run 420) over night when losses were expected to be. The first two runs were run 413 and 415, with different gains, being run 413 at high gain (550 V in the mesh and 1500 V in the cathode that can produce also preamplification) and run 415 at low gain (525 V in the mesh and 1000 V in the cathode). An amplitude and charge cut were applied to select neutrons, as we can see in Figure 25 for those runs. An important detail to observe is the difference in the slopes at low energies (gamma contributions) for both runs as we are operating at different gains. The beam structure is also computed in Figure 26 top. In Figure 26 bottom we show the computed rate of neutrons (in red) when applying the neutron selection. Another two kind of events were selected: in blue are sparks or “recovery from a spark” event and in green uncorrelated neutrons. For run 413, operating at higher gain we had sparks in the event of beam losses as the produced charge was too big for the detector. However, in the case of run 415, when operating at lower gain in both mesh and cathode (closer to the nominal operation conditions), the losses are still clearly identified but no sparks have been produced.

Another interesting plot is comparing the amplitude for runs 414 and 415 (Figure 27). Both runs were taken in same conditions (see Table 7) but in the second one a beam loss was produced. In run 415 we can clearly see the apparition of high amplitude events in the case of beam losses corresponding to the neutrons.

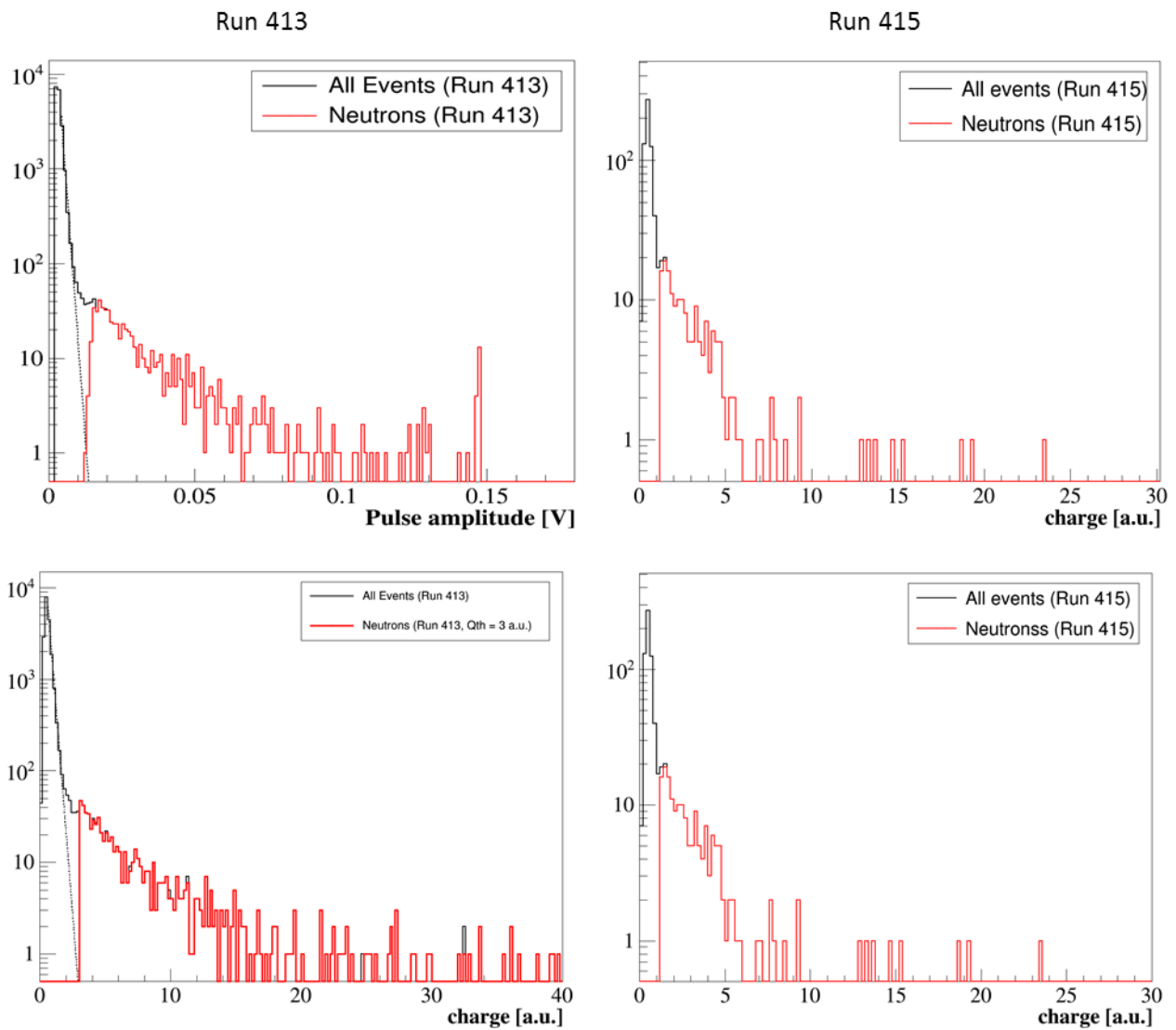


**Figure 25:** (Top) Amplitude distributions for all events (black) and applying the neutron cuts listed in Table 7 (red). (Bottom) Same for the charge distribution.

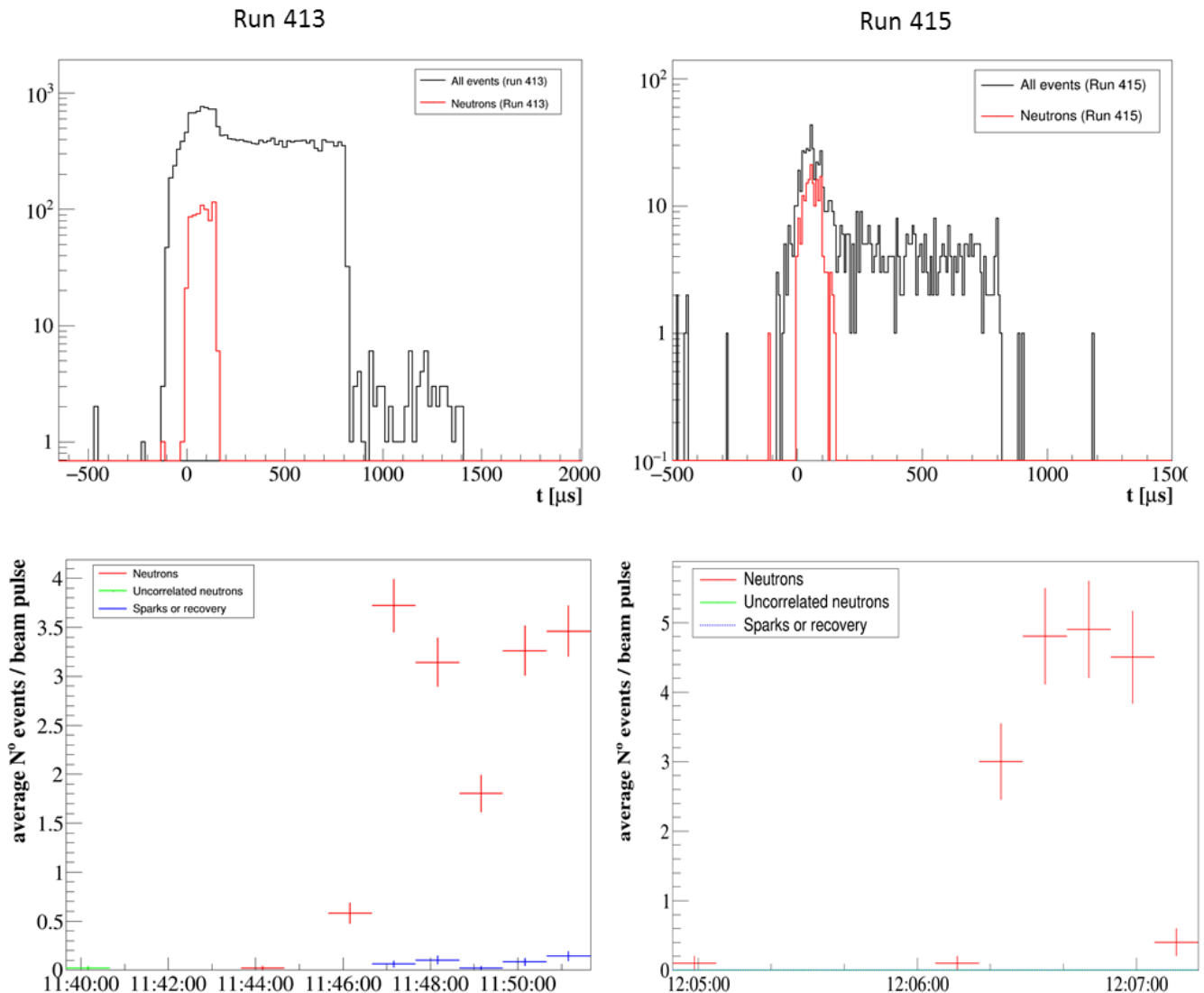


**Figure 26:** (Top) Beam structure for all events (black) and applying the neutron cuts listed in Table 7 (red). (Bottom) Rate of neutrons (red), sparks or “recovery” events (blue) and uncorrelated with the beam neutrons (green) for run 413 and run 415 when applying the neutron cuts.

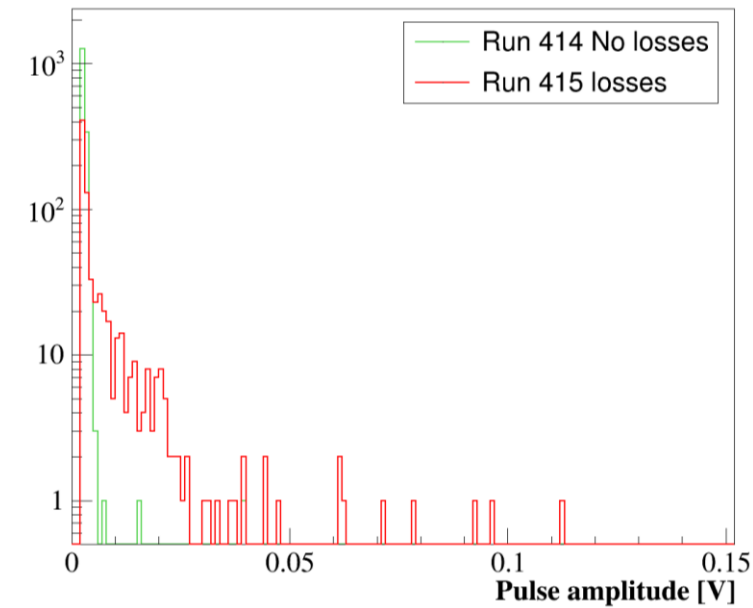


**Figure 27:** Amplitude distribution for two runs operating at same gain. In run 414 no beam losses were produced while in run 415 they were. Although run 414 is 4 times larger than 415, we can clearly see the apparition of high amplitude events in the case of beam losses corresponding to the neutrons.

For run 420, we operate the detector at same gain as in November 2018, 550 V in the mesh and 1500V in the cathode. As we determine in the November 2018 run the cut to select neutrons, we can compare in this case the amplitude, the beam structure and the rate evolution for all events with neutrons (amplitude > 30 mV). We took the data in autotrigger mode and correct later with the trigger to obtain the rate structure. Beam losses were planned to be produced during this run at an unknown time. The rate evolution of all events (*Figure 28*) and of the neutrons (*Figure 29* red) clearly shown an increase at 20:50. A more detailed view is shown in *Figure 29* middle. The losses were indeed produced for 15' between 20:50 and 21:05, as we clearly see. The rate in normal conditions is in average <math>0.005</math> n/pulse while during the loss this average increases to  $\sim 3.5$  n/pulse ( $\sim 1000$  times more) and similar to what we have seen for run 414 and 415. As before, also the sparks and uncorrelated neutrons were selected. Run 420 was also taken at high gain what explains the presence of sparks. However, we can see (*Figure 29* bottom) that the rate of sparks is lower or close to 0 after 21:10, overnight. Before that time and before the sparks, the signal was shared with an IOxOS card and strange crosstalk and effects was observed when operating both systems. So what was identified by sparks are more likely to be large baseline variations.

In *Figure 30*, the beam structure for run 420 is shown in the right. We can see than selecting events with an amplitude > 30 mV the beam size decreases again to what is the proton beam pulse ( $\sim 150\mu\text{s}$ ). We can also see how the rate level is larger during the beam loss over the RF pulse. In green are selected what we have identified as “satellite” neutrons. These events seems to arrive

before the linac 4 trigger. They could be neutrons produced in a previous beam pulse. Further investigations are on-going.

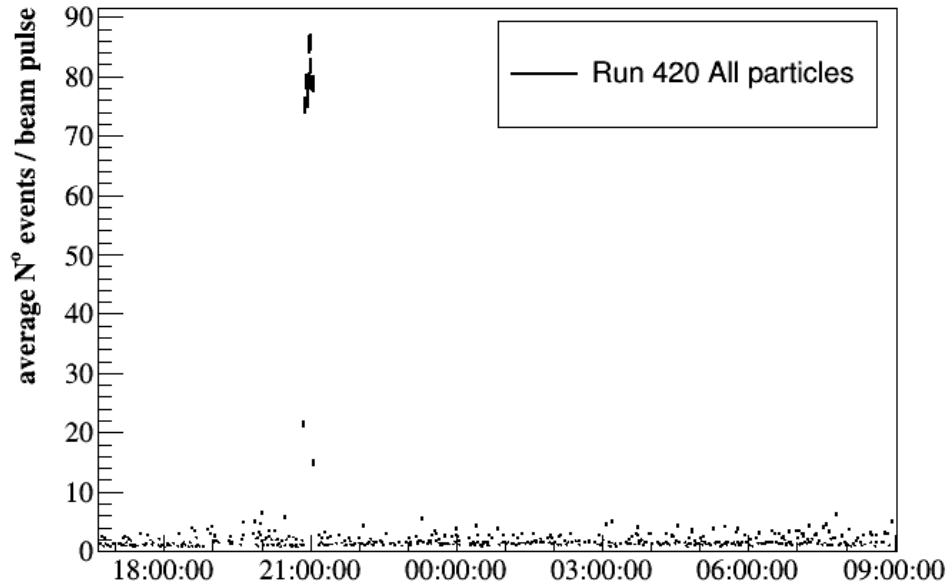


**Figure 28:** Rate of all detected particles for run 420. Beam losses were produced between 20:50 and 21:05.

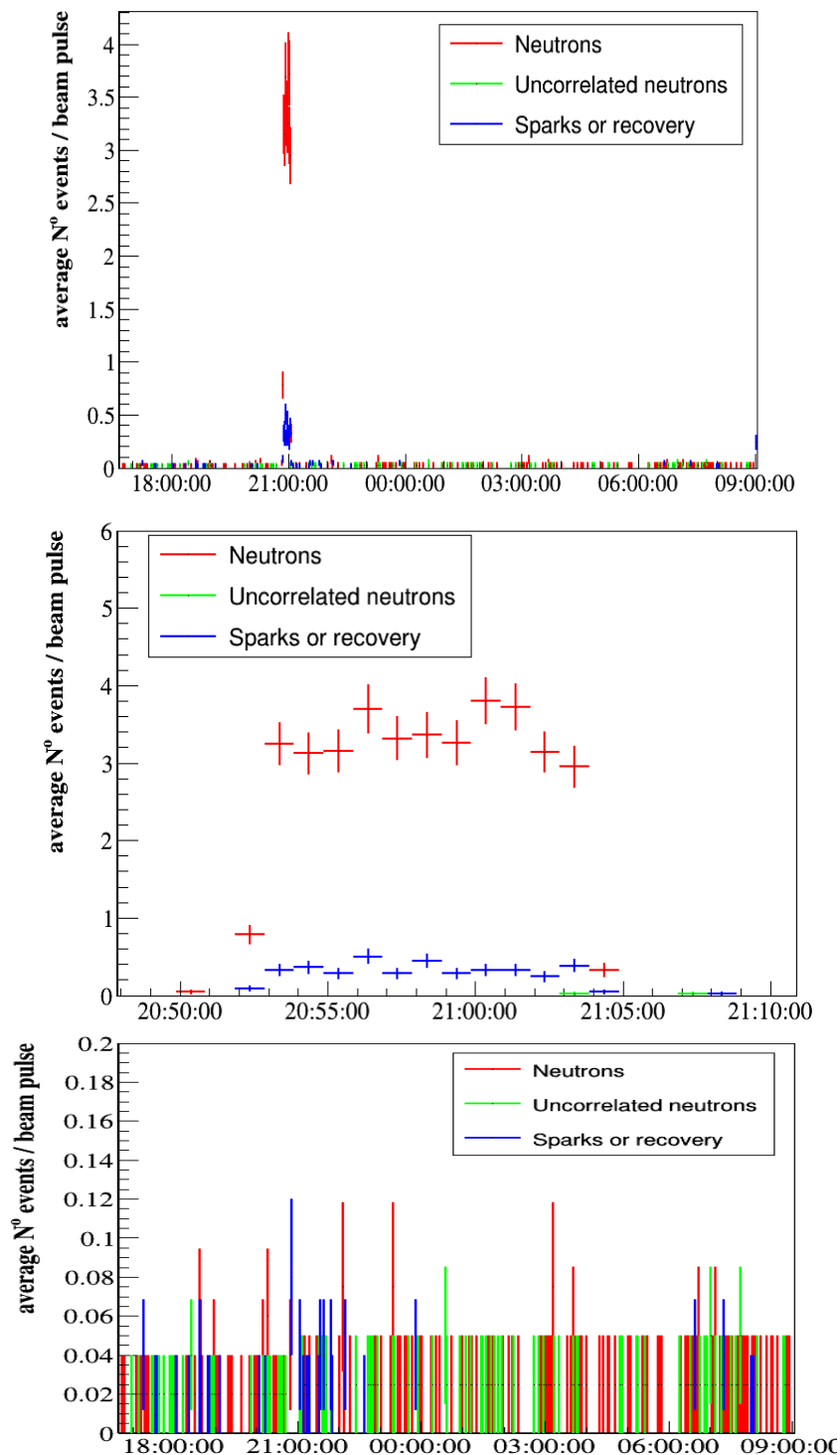


**Figure 29:** (Top) Rate evolution of neutrons events in run 420 (red). (Middle) Same plot zooming in the beam loss times. We can see how the neutron rate is very low and constant over time and increases abruptly at 20:55 time when the losses were produced (the beam was lost between 20:50 and 21:05). In blue the rate of sparks is shown (remember we are operating at very high gain) and in green the rate for uncorrelated neutrons with the beam trigger. (Bottom) Zoom in the low rate part to see in more detail the sparks and uncorrelated neutron rates.

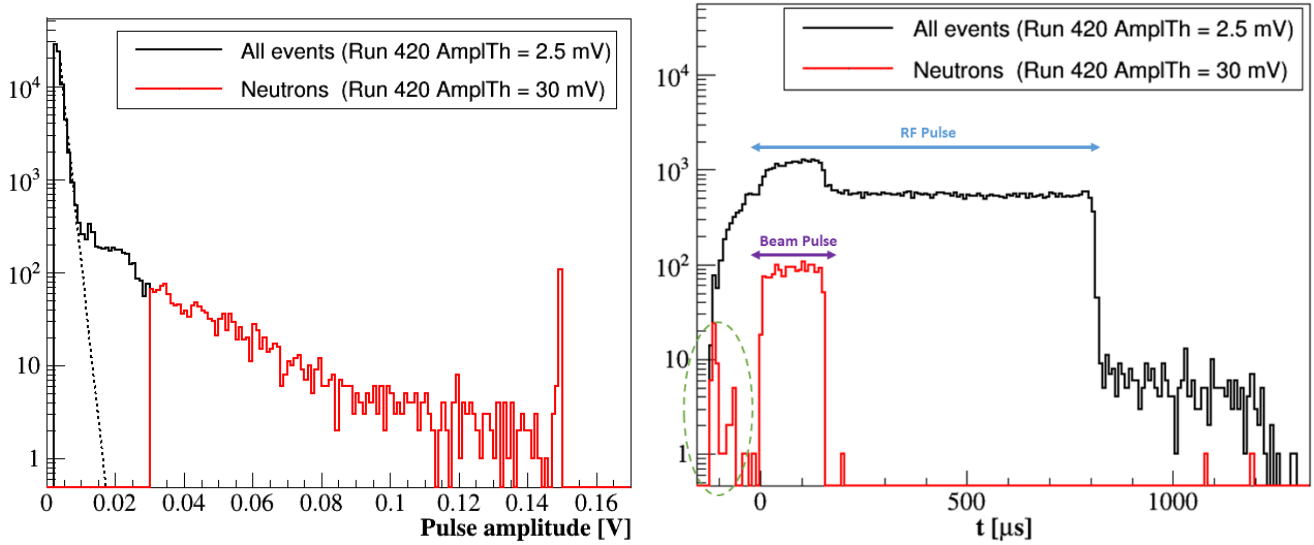


**Figure 30:** Amplitude and beam structure for run 420, when beam losses were forced. We can see that selecting events with an amplitude  $> 30$  mV the beam size decreases again to what is the proton beam pulse ( $\sim 150\mu\text{s}$ ). We can also see how the rate level is larger during the beam loss over the RF pulse. In green are selected what we have identified as “satellite” neutrons as they arrive before the linac 4 trigger. We can see one example in. More details are given in the text.

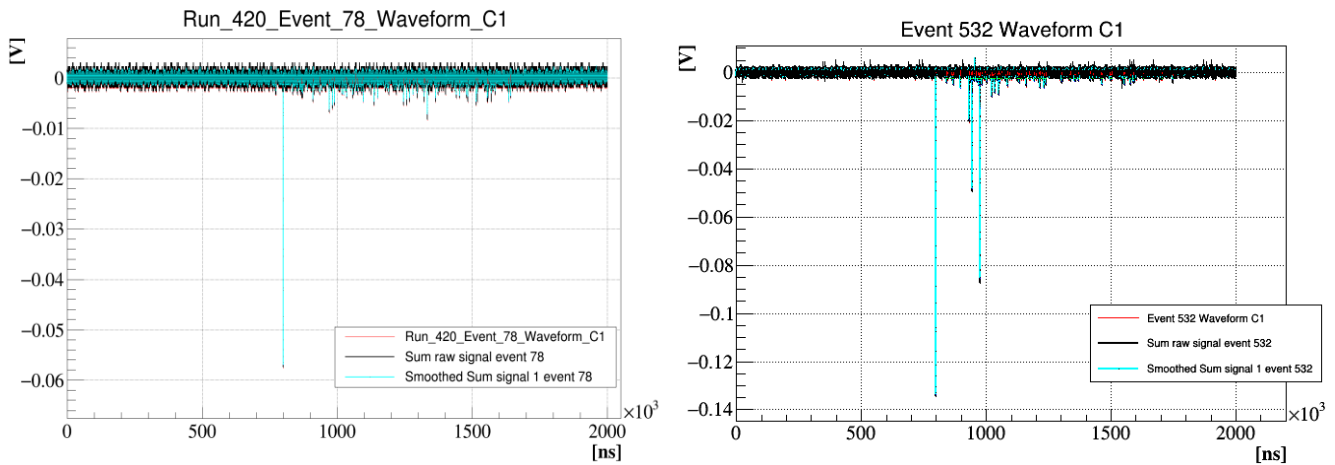
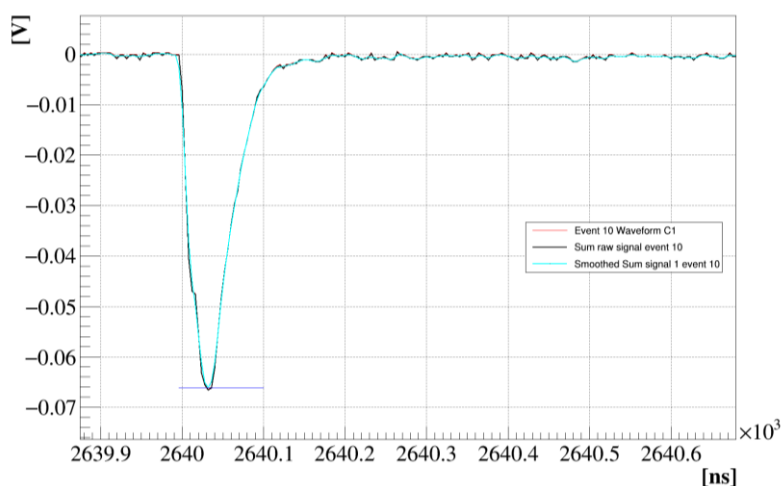


**Figure 31 :** Two of the events populating the green enclosed region of Figure 30. Those events arrive before the linac4 trigger.

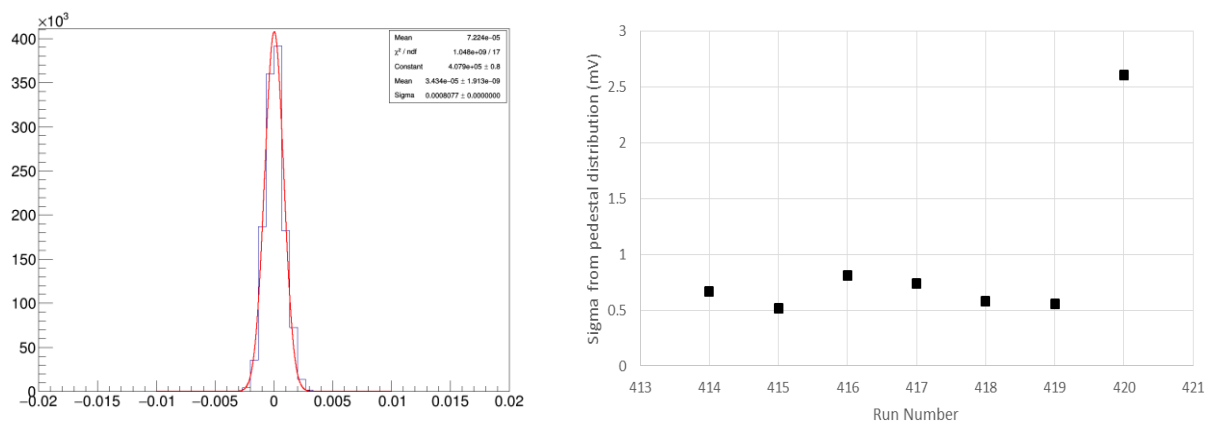
### 7.3.3. FEE response

The response of the FEE card was very satisfactory. **Word about cable/grounding?** The noise level we chose for the analysis was 3 mV and the pedestals had a sigma of 0.5-0.8 mV . A single neutron over the noise level can be seen in Figure 32 and an example of the pedestal distribution as well as the sigma of the pedestal distributions for different runs can be seen in Figure 33.

We have identified some baseline instabilities that corresponded to sparks. These sparks occur in the case of beam losses and when operating at high gain. In these conditions, a high rate will produce a quantity of charge larger than the one the detector can release and therefore, it will produce sparks. A sequence of event, spark, recovery and event is shown in Figure 34.

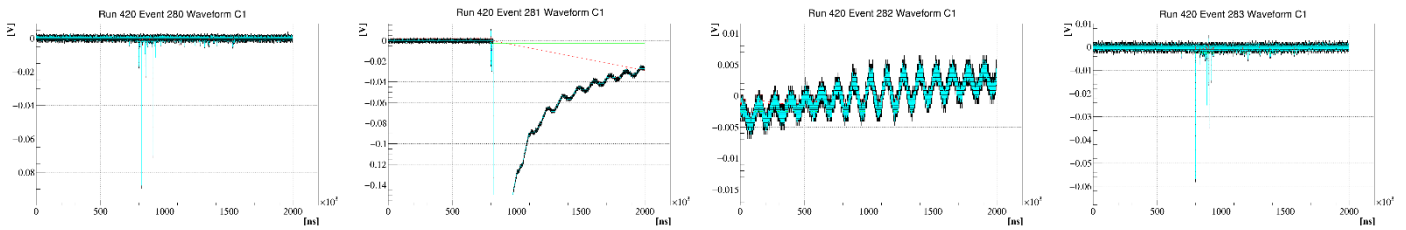


**Figure 32:** Zoom to single neutron to see the S/B ratio.



**Figure 33:** Example of a pedestal distribution for one of the runs taken during the December 2018 campaign (left). (Right) The sigma of the pedestal distributions for different runs. Run 420 was when quite important beam losses were produced and this produced some sparks as explained in the text that broad the pedestal distribution.



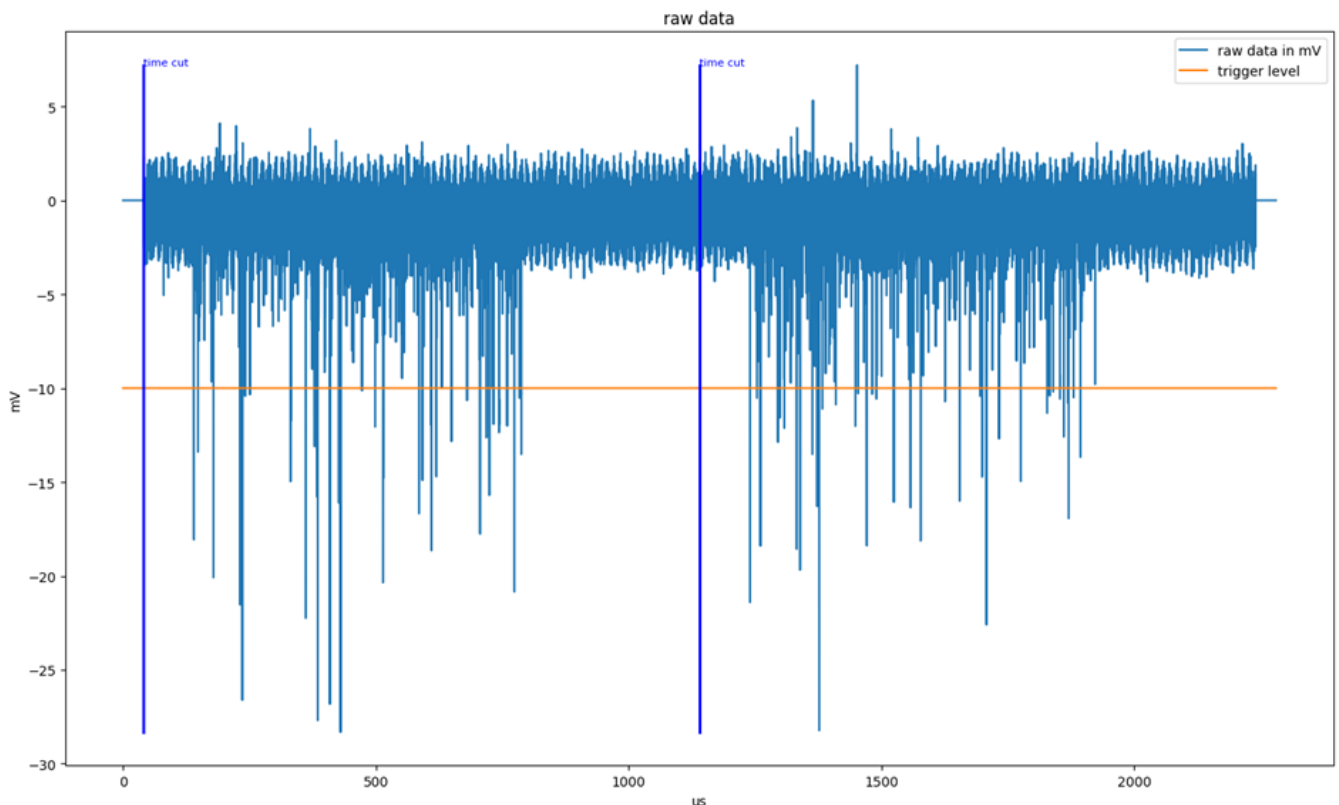


**Figure 34:** In run 420 beam losses were produced as discussed in section 7.3.2. Here we can see some of the sparks produced due to the large quantity of charge produced.



### 7.3.4. DAQ response

During the CERN tests in November 2018, we have tested the FPGA firmware version 0.4. For this we used the executable “mem\_dma\_reader\_tsc” provided by the DMCS partner. This executable made a 3 seconds raw acquisition stored in a file when we ran it. As the pulse was less than 1 Hz, a file could contain 2 pulses.

A python script was prepared to display the data. With a trigger level the python script could concatenate and display interesting sections (see *Figure 35*) (trigger level = -10 mV; pre-trig = 100µs; post-trig = 1000µs). Three runs were done as each time the text file was recorded took about 10’. The goal of the test in any case was to show the capability to record long buffer windows. More results are presented in [6].



**Figure 35:** Raw data acquired at linac4 with and ADC 3111, more details in text.

 	nBLM Project – CDR1.1	CEA-ESS-DIA-RP-0047
	ESS-I	Page 34 sur 40

## 8. HV and LV modules stability

The stability of the HV and LV card have been assessed. We have monitored the channels with and without a load for 24h. We have used 3 nBLM prototypes to load the channels 6 by 6. Operating conditions for the channels, load or no load, are the same:  $V = 400\text{ V}$ ,  $I_{\text{offset}} = 0$  and  $I_{\text{trip}} = 250\mu\text{A}$  after 2 seconds. In addition two longer runs of  $>48\text{ h}$  were taken: one with all the channels unload and one with the channels identified with the largest variations connected to a load.

An example of the monitoring of the voltage and current over time is shown in Figure 38 for 6 channels. The observed variations seems to be constant over a run and change when starting a new run. For each channel in each run the voltage and current distribution have been computed (Figure 39 for the first 6 channels) to obtain the mean value and the sigma of the distribution. The mean value and the sigma of the voltage and current distributions for each channel, when load or unload, are shown in Figure 36 (current) and Figure 37 (voltage).

For the current the sigma is  $\sim 2\text{ nA}$  for most channels. Some channels (4/48) present a larger variation, being the maximum  $10\text{ nA}$  unload. This value decreases to  $8\text{ nA}$  when load. However, a no clear improvement have been measured when loading the channels. The other observation we did is that each channel has a very different offset that will need to be taken into account in the FPGA. Note that the mean values plotted in Figure 36 top are not corrected by the offset.

In the case of the voltage the sigma we obtain for all channels is  $\sim 2\text{ mV}$ . Except for some channels that it goes up to  $20\text{-}25\text{ mV}$ . These more unstable channels have been studied in a longer run of  $>72\text{ h}$  observing that although all channels present the largest variations, 3 of them are characterized by voltage peaks variations of  $3\text{-}4\text{ mV}$  (channel). While representing a small and acceptable variation for our detectors is quite curious and we have contacted CAEN for a possible explanation. Most of these variation have triggered an overcurrent alarm even if the current variation was below the limit imposed of  $250\mu\text{A}$ . This question is also being in discussions with CAEN.

In conclusion, what we have observed is that:

- all current variation is driven by a voltage variation
- We should put the range for the warnings and alarm for a current variation  $> 20\text{ nA}$  once the detector has ramp up its voltage.
- About 3-4/48 channels present larger instabilities.
- Overcurrent alarm trigger in almost all channels from time to time even if the current variation monitored was below the indicated trip current of  $250\mu\text{A}$ .

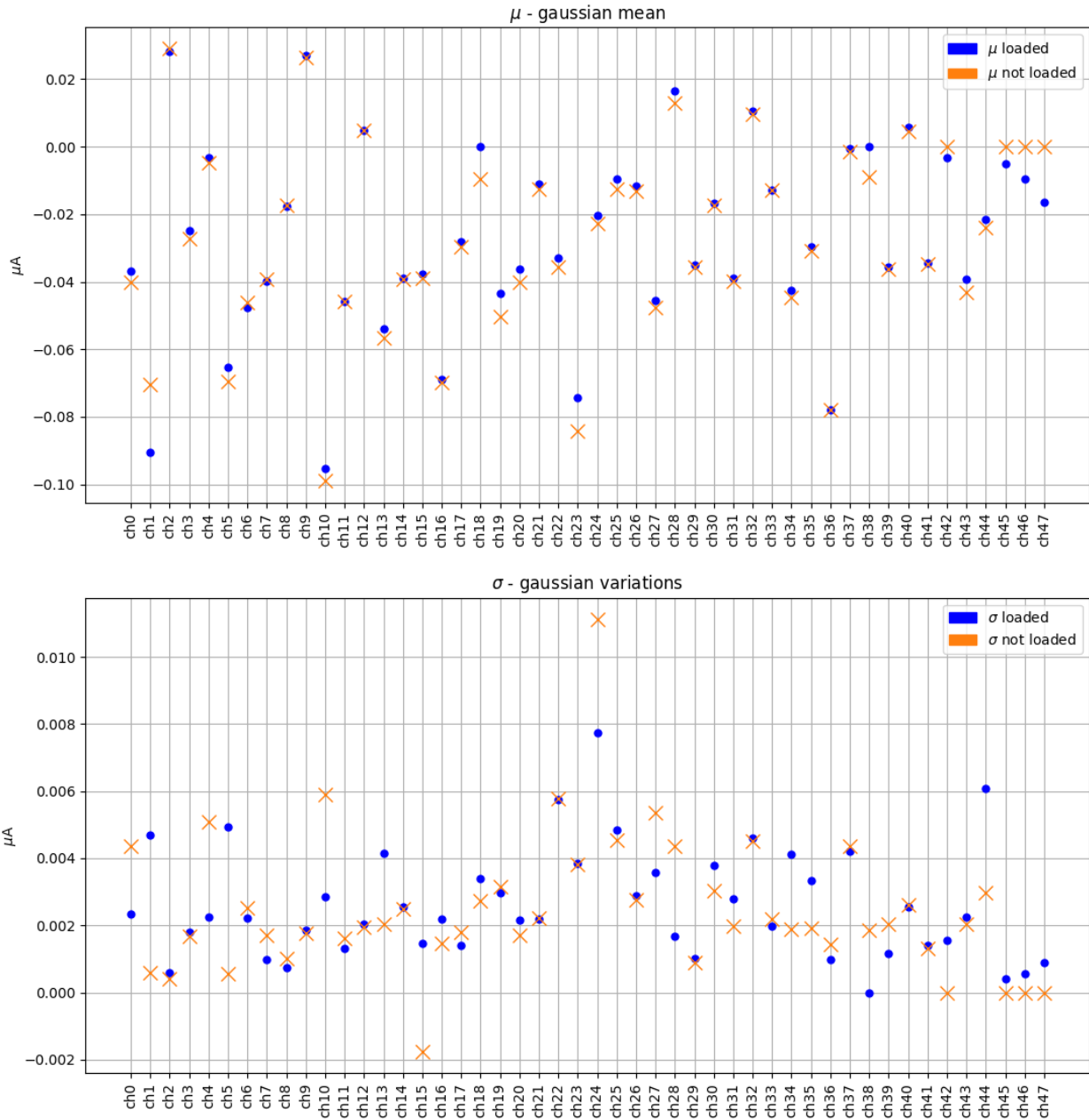


**Figure 36:** Mean (top) and sigma (bottom) of the current distribution for each HV channel when load (blue) or unload (orange). Note that each channel has a different offset and for this reason the meanvalue shown thxxxx

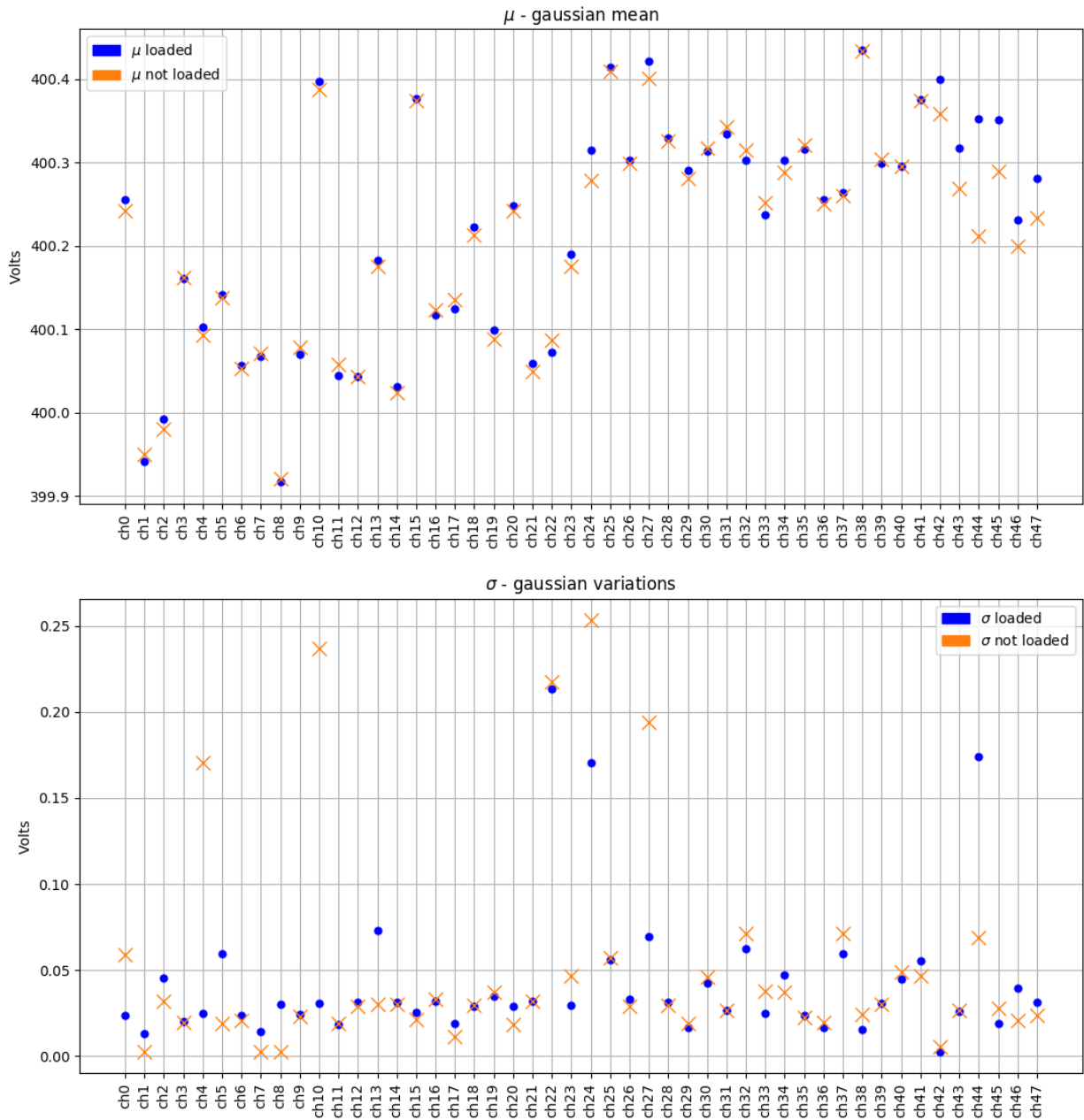


**Figure 37:** Mean (top) and sigma (bottom) of the voltage distribution for each HV channel when load (blue) or unload (orange)

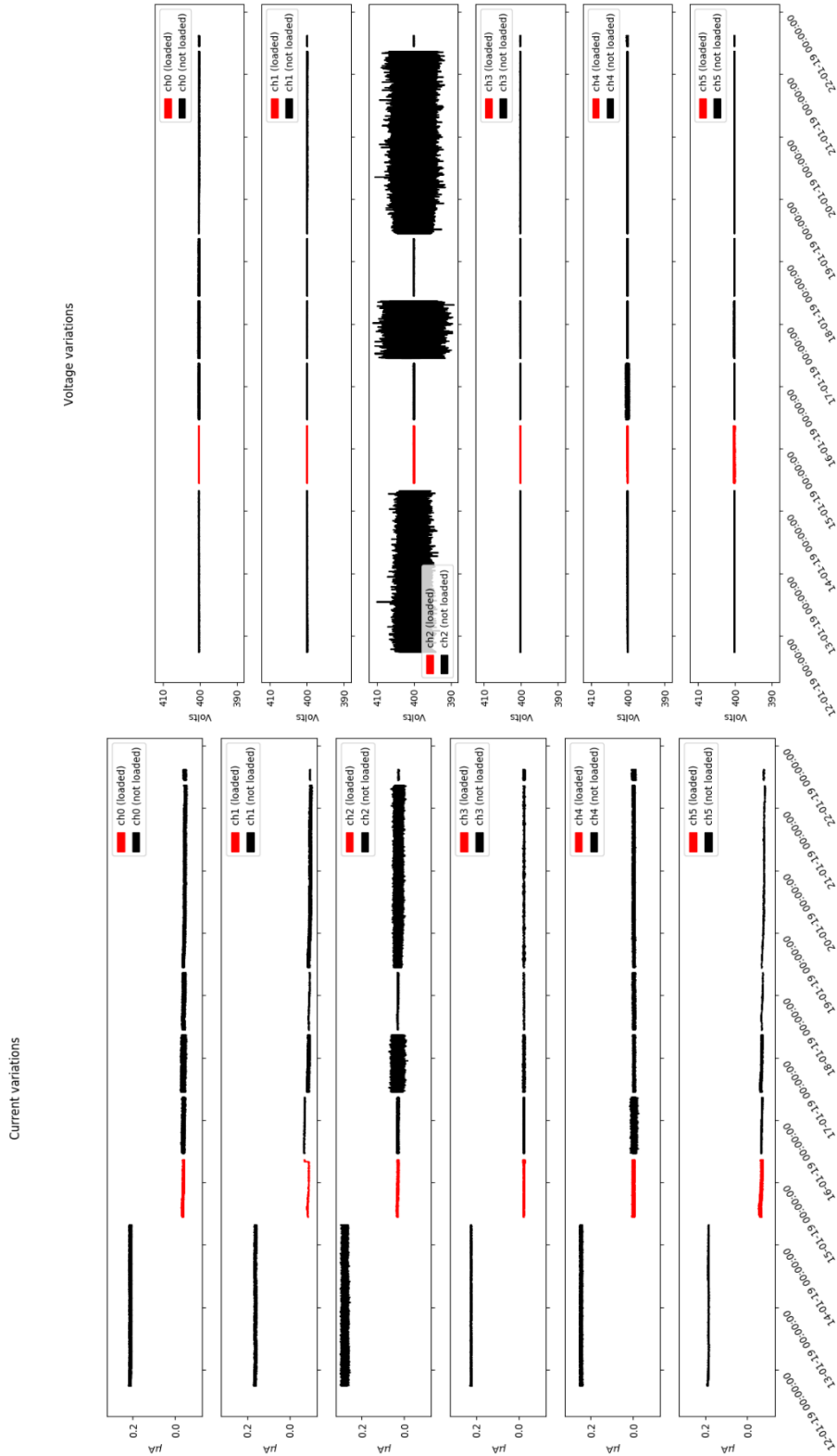
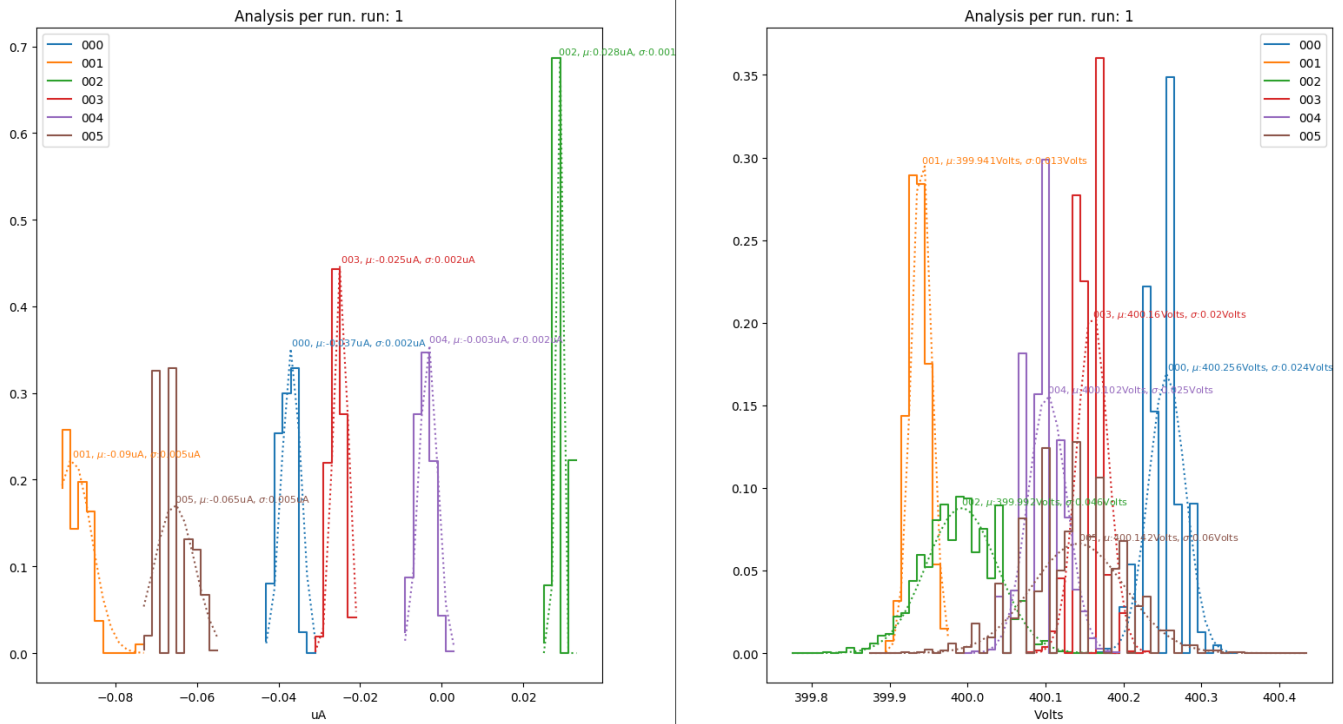
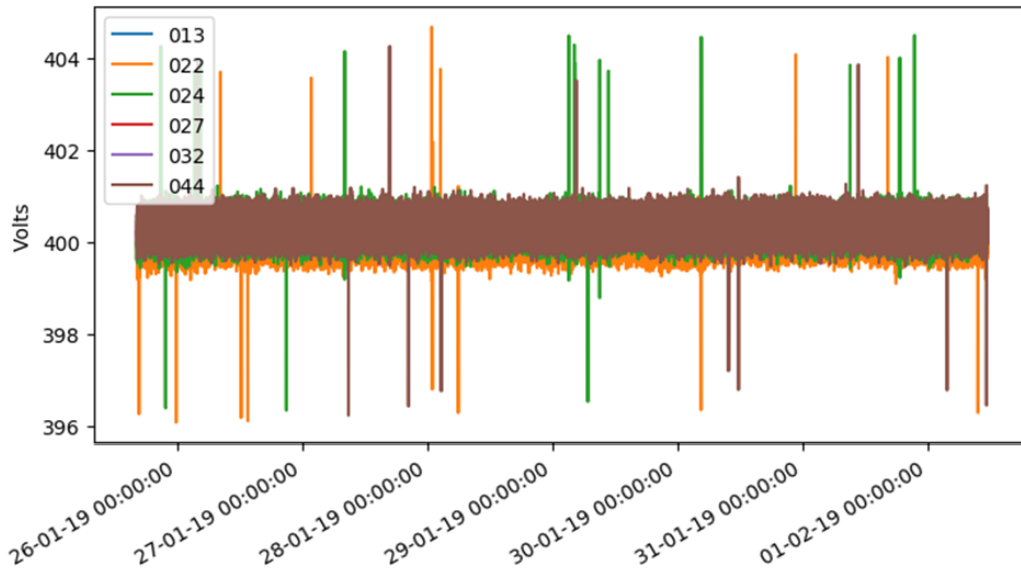


Figure 38 : Evolution of the voltage and current for 6 channels.

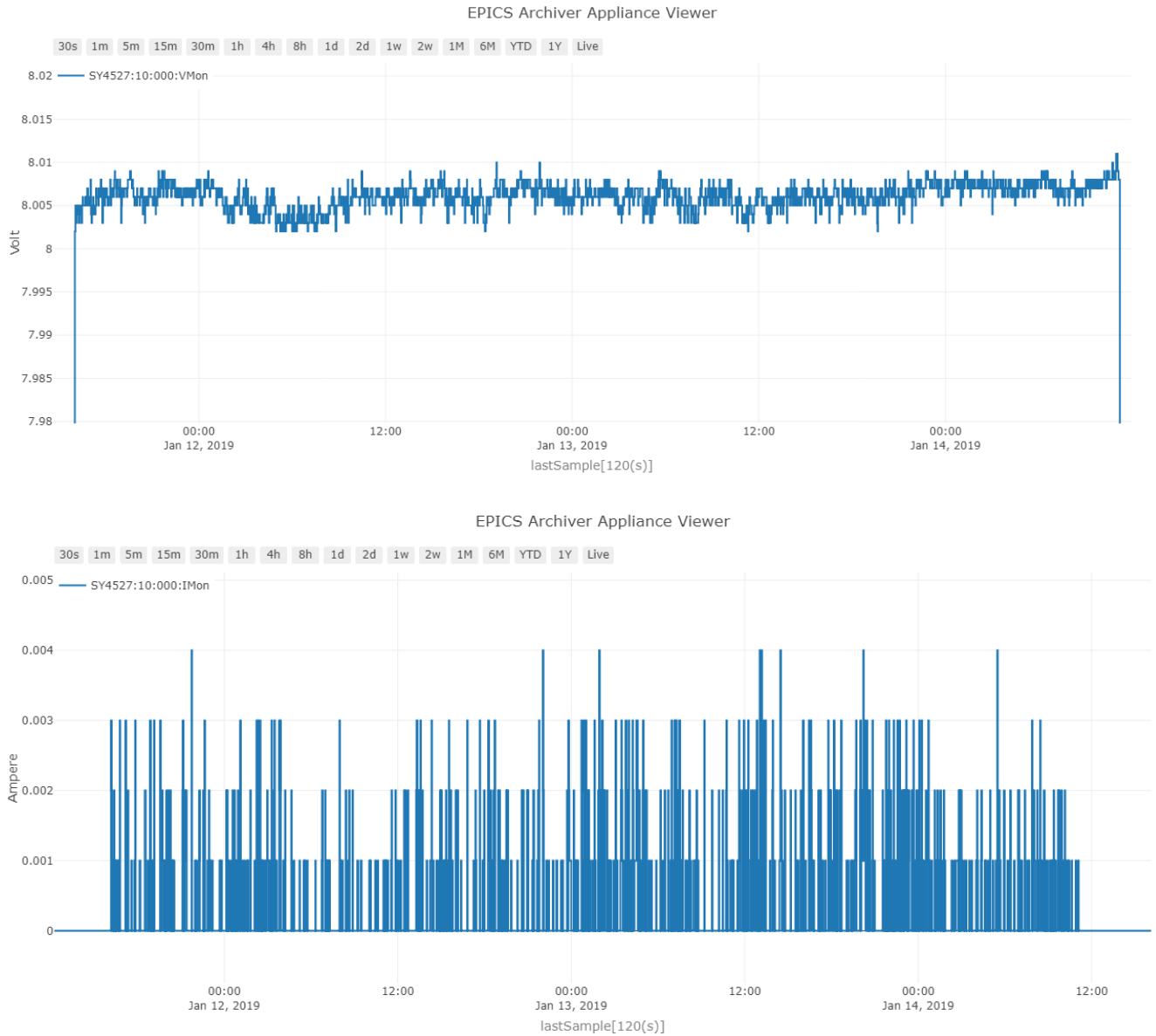


**Figure 39:** Current (left) and voltage (right) distributions for 6 channels (ch0 – ch5) when load as example of the obtained distributions.





**Figure 40:** Evolution of the monitored voltage for the identified as worst channels in previous runs. Although all present the largest variations, 3 of them are characterized by voltage peaks variations of 3-4 mV. While representing a small and acceptable variation for our detectors is quite curious and we have contacted CAEN for a possible explanation. Most of these variation have triggered an overcurrent alarm even if the current variation was below the limit imposed of 250 μA. This question is also being in discussions with CAEN.

The LV card have been also monitored. However, this has been a partial test as it has been tested without a load for the moment. In Figure 41 we can see the evolution of the monitored voltage and current in when applying an initial voltage of 8 V. Tests will be repeated with a FEE card connected in the near future.



**Figure 41:** Voltage and current from the LV A2519 card monitored over time without a load connected.

 	nBLM Project – CDR1.1	CEA-ESS-DIA-RP-0047
	ESS-I	Page 40 sur 40

## REFERENCES

- [1] L. Segui et al, “nBLM PDR1.2,” CEA-ESS-DIA-RP-0027, 2017.
- [2] L. Segui, «nBLM Detectors Experimental Results,» <https://indico.esss.lu.se/event/1083/>, July 2018.
- [3] L. Segui et al, “PDR1.1,” CEA-ESS-DIA-RP-0013, (ESS-0110762), 2016.
- [4] L.Segui, «Modes covered by the nBLM system,» <https://indico.esss.lu.se/event/948/>, December 2017.
- [5] L. Segui, «Monte Carlo results: nBLM response to EES,» ESS-0107320 / CEA-ESSDIA-RP-0023, July 2017.
- [6] I. D. Kittlemann, «Preliminary results of the ESS nBLN DAQ tests at Linac4,» <https://indico.esss.lu.se/event/1173/>, February 2019.